

Studies of Respiratory Rhythm Generation Maintained in Organotypic Slice  
Cultures

Wiktor Samuel Phillips

Williamsburg, Virginia

Bachelor of Science, College of William & Mary, 2010

A Dissertation presented to the Graduate Faculty  
of the College of William and Mary in Candidacy for the Degree of  
Doctor of Philosophy

Department of Applied Science

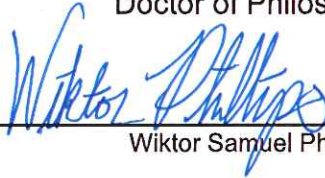
The College of William and Mary  
January, 2017



APPROVAL PAGE

This Dissertation is submitted in partial fulfillment of  
the requirements for the degree of

Doctor of Philosophy



---

Wiktor Samuel Phillips

Approved by the Committee, November, 2016



---

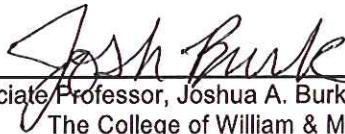
Committee Chair

Professor, Christopher Del Negro, Applied Science  
The College of William & Mary



---

Associate Professor, Jens Christian Rekling, Neuroscience & Pharmacology  
University of Copenhagen



---

Associate Professor, Joshua A. Burk, Psychology  
The College of William & Mary



---

Associate Professor, Hannes Schriepp, Applied Science  
The College of William & Mary

## COMPLIANCE PAGE

Research approved by

Institutional Animal Care and Use Committee (IACUC)  
The College of William & Mary

Protocol number(s): (1) IACUC-2010-07-12-6795-cadeln  
(2) IACUC-2013-07-12-8828-cadeln  
(3) IACUC-2013-07-10-8833-cadeln  
(4) IACUC-2014-03-12-9412-cadeln  
(5) IACUC-2016-08-02-11305-cadeln  
(6) IACUC-2016-08-02-11302-cadeln

Date(s) of approval: (1) 2010-07-30  
(2) 2013-07-19  
(3) 2013-07-29  
(4) 2014-04-16  
(5) 2016-08-17  
(6) 2016-08-17

## ABSTRACT

Breathing is an important rhythmic motor behavior whose underlying neural mechanisms can be studied *in vitro*. The study of breathing rhythms *in vitro* has depended upon reduced preparations of the brainstem that both retain respiratory-active neuronal populations and spontaneously generate respiratory-related motor output from cranial and spinal motor nerves. Brainstem-spinal cord *en bloc* preparations and transverse medullary slices of the brainstem have greatly improved the ability of researchers to experimentally access and thus characterize neurons important in respiratory rhythmogenesis. These existing *in vitro* preparations are, however, not without their limitations. For example, the window of time within which experiments may be conducted is limited to several hours. Moreover, these preparations are poorly suited for studying subcellular ion channel distributions and synaptic integration in dendrites of rhythmically active respiratory neurons because of tortuous tissue properties in slices and *en bloc*, which limits imaging approaches. Therefore, there is a need for an alternative experimental approach. Acute transverse slices of the medulla containing the preBötzinger complex (preBötC) have been exploited for the last 25 years as a model to study the neural basis of inspiratory rhythm generation. Here we transduce such preparations into a novel organotypic slice culture that retains bilaterally synchronized rhythmic activity for up to four weeks *in vitro*. Properties of this culture model of inspiratory rhythm are compared to analogous acute slice preparations and the rhythm is confirmed to be generated by neurons with similar electrophysiological and pharmacological properties. The improved optical environment of the cultured brain tissue permits detailed quantitative calcium imaging experiments, which are subsequently used to examine the subcellular distribution of a transient potassium current,  $I_A$ , in rhythmically active preBötC neurons.  $I_A$  is found on the dendrites of these rhythmically active neurons, where it influences the electrotonic properties of dendrites and has the ability to counteract depolarizing inputs. These results suggest that excitatory input can be transiently inhibited by  $I_A$  prior to its steady-state inactivation, which would occur as temporally and spatially summing synaptic inputs cause persistent depolarization. Thus, rhythmically active neurons are equipped to appropriately integrate the activity state of the inspiratory network, inhibiting spurious inputs and yet yielding to synaptic inputs that summate, which thus coordinates the orderly recruitment of network constituents for rhythmic inspiratory bursts. In sum, the work presented here demonstrates the viability and potential usefulness of a new experimental model of respiratory rhythm generation, and further leverages its advantages to answer questions about active currents in dendrites that could not previously be addressed in the acute slice model of respiration. We argue that this new organotypic slice culture will have widespread applicability in studies of respiratory rhythm generation.

# TABLE OF CONTENTS

Acknowledgements	ii
Dedication	iii
List of Figures	iv
Introduction	1
CHAPTER 1: Organotypic slice cultures containing the preBötzinger complex generate respiratory-like rhythms	
1.1 Introduction	17
1.2 Results	19
1.3 Discussion	30
1.4 Methods	36
1.5 References	42
CHAPTER 2: Dendrites of rhythmically active neurons in the preBötzinger complex contain an $I_A$ -like potassium current	
2.1 Introduction	45
2.2 Results	48
2.3 Discussion	62
2.4 Methods	69
2.5 References	76
Conclusions	79

## ACKNOWLEDGEMENTS

Christopher del Negro gave me both an opportunity and sense of direction. He pushed me, demanded excellence, and kindled a discipline for my craft. Without his help, patience and support through my years spent both at home and abroad, none of this would have been possible.

Jens C. Rekling has been an invaluable mentor. He both welcomed and actively encouraged creative problem solving and novel ways of thinking about physiology. The result was a fervent interest in the science. Perhaps most importantly I consider him a good friend, both trustworthy and sage. Thanks for helping me—perhaps even unknowingly—really enjoy what I do, Jens.

My parents have been ever-loving and supportive of me. Helping me in times of need over and over again, all while hardly ever seeing me for the past three years. I owe them an enormous debt of gratitude.

I also wish to thank my wife, Saoussane, for having the patience and strength to endure long periods of being away from each other while I worked towards finishing my dissertation project. And also for putting up with a husband that yammers constantly about science! I know—professional nerd.

The many conversations I shared with Henrik Jahnsen (while chewing bread and jam on Thursday mornings) were both insightful and helpful. Henrik's advice taught me how to be a better electrophysiologist and also how to be very critical of science—both my own and others'.

I wish to thank Dr. Hannes Schniepp and Dr. Joshua Burk for taking valuable time away from their schedule to carefully scrutinize the body of work presented herein.

Lastly, I wish to thank the administrative staff at the College of William & Mary that have always been absolutely superb. None of us would ever have gotten anything done without Rosi, Lydia and Lianne there to set us straight.

This dissertation is dedicated to my family and  
dearest friends, both near and far away.

## LIST OF FIGURES

I.1.	The <i>in vitro</i> slice preparation of the preBötzing complex	3
I.2.	The semiporous membrane organotypic culture preparation	7
1.1.	Oscillatory calcium activity in three different transverse brainstem slice preparations	20
1.2.	Propagation of calcium activity in brainstem slice cultures and brainstem-cerebellar co-cultures	23
1.3.	Low and high magnification views of oscillatory activity	24
1.4.	Retrograde labeling of neurons following local co- iontophoresis of biocytin and KCl in roller-drum cultures	26
1.5.	Simultaneous imaging of GFAP <sup>+</sup> cells expressing EGFP and time-series of fluorescent calcium activity	27
1.6.	Whole-cell patch clamp recordings from a rhythmically active neuron in the ventral oscillatory group of a brainstem-cerebellar co-culture after 7 days-in-vitro	29
2.1.	Electroresponsive properties of oscillating <i>type-1</i> and <i>type-2</i> neurons	49
2.2.	Bath applied 4-aminopyridine increases dendritic Ca <sup>2+</sup> transients in response to ramp depolarizations	52
2.3.	Dendritic iontophoresis of Cd <sup>2+</sup> reduce dendritic Ca <sup>2+</sup> -transients evoked by current pulses	57
2.4.	Dendritic iontophoresis of 4-aminopyridine increases dendritic Ca <sup>2+</sup> transients evoked by action potentials	60
C.1.	Adeno-associated viral transduction of red fluorescent protein in slice cultures containing the preBötzing complex	

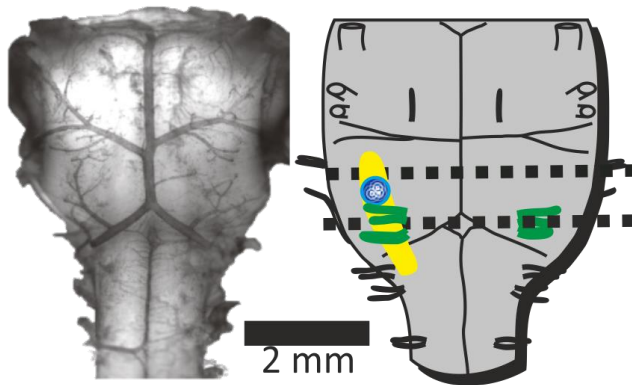
## INTRODUCTION

Our understanding of the neural mechanisms for breathing has advanced exponentially because of studies exploiting reduced *in vitro* preparations, which broaden the scope of feasible experiments by providing a tractable laboratory model of the behavior (respiration). *In vitro* breathing models retain core brain circuitry necessary for the production of respiratory-related rhythms while improving access to neuronal populations of interest for recording and (in some cases) manipulation. Respiratory rhythmogenesis has been studied *in vitro* using acute brainstem-spinal cord and medullary slice preparations for more than 30 years (Funk and Greer, 2013; Smith et al., 1991; Suzue, 1984). Despite their numerous advantages, these preparations are not amenable to some contemporary viral transfection techniques nor imaging methodologies. Acute preparations containing respiratory neural circuits are poorly suited for these methods because they remain only viable for hours, whereas viral transfection can take days. Also, acute slices are hundreds of microns thick and even the most sophisticated imaging methods are not practicable at depths exceeding 100  $\mu\text{m}$  (at the most), which forecloses our ability to measure the majority of respiratory neurons (or glia) at depths that exceed 100  $\mu\text{m}$ . In contrast, organotypic culture models of respiratory rhythm generation may provide an alternate rhythmically active platform suited to long-term experimentation and imaging (on the order of

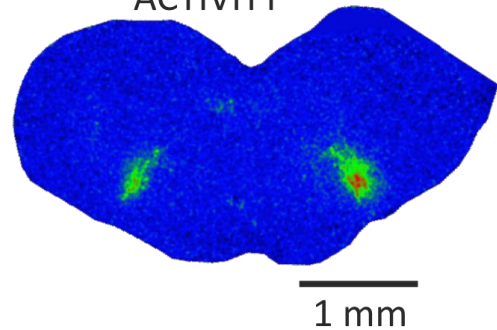
days and weeks), allowing for a new array of techniques to investigate the biophysical mechanisms giving rise to the respiratory rhythm.

Throughout the 1980s, mammalian respiration was studied primarily *in vivo* using decerebrate cats (Eldridge et al., 1976, 1981; Foutz et al., 1989; Pierrefiche et al., 1994; Ramirez et al., 1998; Richter, 1982; Schwarzacher et al., 1995; Smith et al., 1989). The study of respiratory rhythm *in vivo* suffered from an inability to precisely control the recording milieu, and required the use of anesthetics such as pentobarbital, which significantly enhance the strength of chloride-mediated synaptic inhibition (thus changing the network properties). Reduced *in vitro* preparations that preserved respiratory rhythm-generating functionality were developed using neonatal rodents, beginning with the brainstem-spinal cord *en bloc* preparation (Smith and Feldman, 1987; Smith et al., 1990; Suzue, 1984). *In vitro* preparations were further reduced through a series of serial transections that identified the location of the preBötzinger complex (preBötC)--the core rhythm-generating network necessary for inspiratory-related motor output (Smith et al., 1991). Transverse slices of the medulla containing the preBötC, which also retain respiratory related hypoglossal (XII) motoneurons and premotor neurons, produce a bilaterally synchronized rhythm that can be monitored as motor output from the hypoglossal cranial nerve rootlets that are also captured in the slice (Figure I.1). If properly sectioned (Ruangkittisakul et al., 2006, 2011, 2014), the rostral surface of these slices exposes neurons in the preBötC for detailed recording experiments, and for over 25 years acute transverse slices containing the preBötC have been utilized to define the behavior, membrane properties, synaptic connectivity, and

## BRAINSTEM FROM NEWBORN MOUSE



## FLUO-8,AM LOADED SLICE CYCLE TRIGGERED AVERAGE OF PBC ACTIVITY



## SLICE PREPARATION

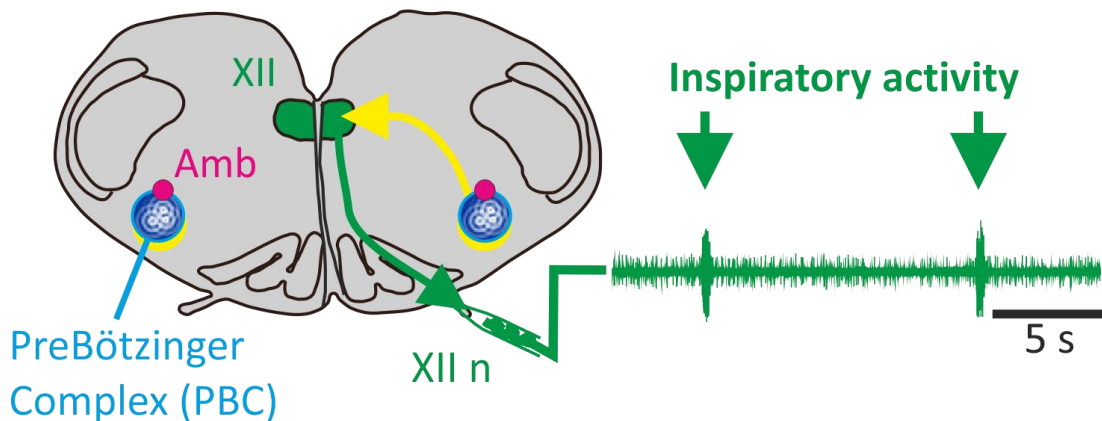


**Figure I. 1** The *in vitro* slice preparation of the preBötzing complex. *Top-left panel:* brainstem of a newborn mouse and diagram showing the rostral and caudal locations of slice transection (dotted lines). *Top-right panel:* Cycle-triggered average of preBötC bilaterally synchronized rhythmic calcium activity imaged using the membrane-permeable fluorescent calcium indicator dye, Fluo-8AM. Green and red areas correspond to active regions in the slice. *Bottom-left panel:* a schematic diagram of the slice, showing locations of the bilateral preBötC, nucleus ambiguus (Amb), hypoglossal motor nucleus (XII) and hypoglossal cranial nerve rootlet (XII n). *Bottom-right panel:* respiratory-related motor output recorded through a suction electrode on XII n.

genetic identity of interneurons involved in respiratory rhythmogenesis (Bouvier et al., 2010; Feldman et al., 2013; Gray et al., 1999; Rekling et al., 1996). However, this acute slice preparation has inherent limitations. Acute slice preparations are at best useful for several hours (Funk and Greer, 2013), precluding chronic pharmacological experiments or the use molecular techniques requiring long incubation periods (e.g., viral transfection). They are also poorly suited for

assaying subcellular distributions of ionic membrane conductances or synaptic integration occurring in dendrites.

In other regions of the brain, the integrative properties of dendrites have been studied via direct dendritic patch-clamp or via quantitative imaging of fluorescent calcium and voltage indicators (Stuart and Spruston, 2015). However, dendrites of rhythmically active interneurons in the preBötC are relatively thin (~1-2  $\mu\text{m}$  diameter) and although their branch structure is remarkably planar, they extend ~37  $\mu\text{m}$  in the parasagittal plane on average (Picardo et al., 2013), which is enough to make them difficult to target for dendritic patch-clamp. Dendrites that traverse the z-axis are also more difficult to quantitatively image since less of the branching structure can be captured within a single focal plane. Lastly, neurons in the preBötC that are visualized most easily for both whole-cell patch-clamp and imaging are found near the surface of the slice (<100  $\mu\text{m}$  depth). Neural processes that traverse the z-axis near the surface are inherently prone to lesioning during slice-cutting procedures, which may compromise measurements. Limitations to the investigation of dendritic properties in acute slices have thus limited our ability to discover excitable properties of preBötC neurons beyond the peri-somatic area. Indirect observations suggest integrative events occur on dendrites (Morgado-Valle et al., 2008; Pace and Del Negro, 2008; Pace et al., 2007a), and dendritic activity in rhythmically active neurons of the preBötC has been observed and measured (Del Negro et al., 2011). However, the manner in which integrative events in dendrites operate in a rhythmogenic context is still poorly understood. Similarly, the distribution of voltage-gated ion channels on dendrites outside the

peri-somatic area is unknown, which may additionally influence synaptic integration in the context of respiratory rhythm generation.

Dendrites likely play an important role in inspiratory burst generation due to the involvement of dendritically-localized integrating conductances (Del Negro et al., 2011; Pace and Del Negro, 2008; Pace et al., 2007a). Respiratory rhythm generation relies on synaptic excitatory input and is an emergent property of the preBötC network (Del Negro et al., 2002; Pace et al., 2007b). The group-pacemaker mechanism attempts to explain emergent network rhythm as an interplay between intrinsic membrane conductances and recurrent excitation among interconnected neurons in the preBötC. In a feed-forward process, these neurons generate a building amount of temporally-summed synaptic input. Rhythmically active neurons then amplify summated excitatory input into bursts of action potentials at the soma. The intrinsic membrane conductance responsible for the amplification of excitatory input has been identified as a calcium-activated non-specific cation current ( $I_{CAN}$ ) (Beltran-Parrazal et al., 2012; Pace and Del Negro, 2008; Pace et al., 2007a), and is modulated by metabotropic glutamate receptors (mGluRs) (Pace and Del Negro, 2008). As such, recruitment of  $I_{CAN}$  likely occurs at the point of synaptic input—the dendrites. Synaptic integration occurring in dendrites can greatly influence the behavior of neurons. Voltage-dependent ion channels have been found in dendrites in nearly every mammalian neuron tested (Stuart and Spruston, 2015; Stuart et al., 2016). Depending on their exact subcellular distribution, such currents can influence the amplitude and summation of EPSPs (Magee, 2000), and in some cases support back-propagating action

potentials or calcium spiking (Kampa and Stuart, 2006; Larkum et al., 1999; Otsu et al., 2014). These phenomena allow neurons to alter their output behavior depending on the strength and timing of excitatory input (Bittner et al., 2015; Gidon and Segev, 2012; Larkum et al., 2001; Poirazi et al., 2003).

The inability to both conduct long-lasting experiments and thoroughly investigate subcellular properties might be ameliorated by the use of organotypic slice cultures. Organotypic slice cultures preserve slices of central nervous system tissue in an incubated culture environment such that the projections between regions contained in the slice and synaptic connectivity of local microcircuits are grossly retained over time. Slice cultures can be produced in one of two ways: the Gähwiler roller-tube method (Gähwiler, 1981, 1988), or the Stoppini semi-permeable membrane method (Stoppini et al., 1991). These techniques differ in their means of oxygenating brain slices. The roller-tube method depends on a slowly rotating (~5 rpm) drum that allows cover glass-mounted brain slices to be alternatively exposed to media and air. The Stoppini method utilizes semi-permeable membranes on which slices remain stationary. Membrane cultures maintain a thin layer of media at the tissue surface that allows oxygenation via passive diffusion (Figure 1.2). In both methods, slices of CNS tissue can be maintained *in vitro* for up to eight weeks (Humpel, 2015). Thus the duration of experiments can be expanded from a single day to many weeks, including multiple recording sessions (Dong and Buonomano, 2005; Jahnsen et al., 1999; Seidl and Rubel, 2010; Yamamoto et al., 1997). The longevity of organotypic cultures permits targeted transfections and subsequent expression of vectors in one or many cells

(Arsenault et al., 2014; Forsberg et al., 2016; Murphy and Messer, 2001; Nguyen et al., 2012; Rathenberg et al., 2003; Wickersham et al., 2007). They have also been used as models for chronic exposure treatments (Laake et al., 1999; Newell et al., 1995; Peña, 2010; Rytter et al., 2003).

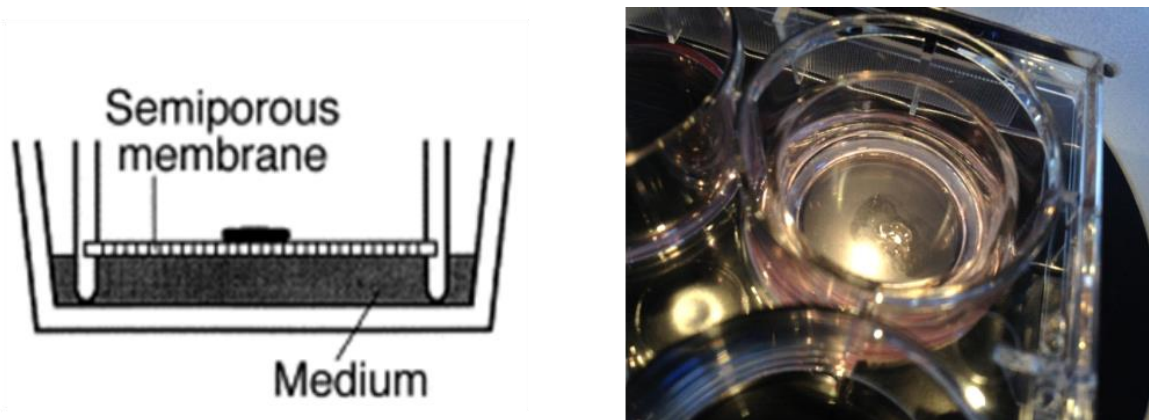


**Figure 1. 2** The semiporous membrane organotypic culture preparation. *Left panel:* diagram of a slice placed on top of a semiporous membrane insert. Note the insert elevates the slice in the well so it does not become submerged. A thin layer of medium is maintained over the slice to prevent dessication. *Right panel:* image of a slice culture after 14 days-in-vitro.

One of the early applications of slice cultures was the study of developing neuronal processes (Muller et al., 1993; Zhabotinski et al., 1979; Zimmer and Gähwiler, 1987). Neurons lesioned during slicing of brain tissue either die or regenerate their neurites in cultures (Stoppini et al., 1993). As such, there is a greater likelihood that the dendrites and axons of neurons are intact when they are targeted for recording in slice cultures. The extent to which regenerated dendrites recapitulate the properties of neurons *in situ* or *in vivo*, can thus be tested. A byproduct of the culturing process is a gradual flattening-out of the slice and a concomitant increase in the clarity of the tissue (Guy et al., 2011; Humpel, 2015). As a result, the distance between synaptic partners is reduced in the z-axis, causing dendrites to become more planar. In sum, the properties of organotypic slice cultures appear to address

the issues preventing long-duration experiments and the investigation of sub-cellular dynamics. Further, organotypic culture models have already proven successful for studying spinal cord motor rhythms (Czarnecki et al., 2008; Darbon et al., 2003; Magloire and Streit, 2009; Tschertter et al., 2001), and may thus be equally suited for patterns emerging from brainstem respiratory networks. Such precedence and increased experimental flexibility has motivated the development of a novel model of respiratory rhythmogenesis described herein.

In Chapter 1, a novel organotypic slice culture containing the preBöttinger complex is described. The spatiotemporal dynamics of rhythmic network behavior is compared to acute slices via whole-slice calcium imaging, including responses to well-established modulators of respiratory rhythm (Gray et al., 1999). We confirm that the rhythm in the culture results from the preBötC neuronal network by measuring the time course of calcium transients occurring in fluorescently labelled astrocytes versus neurons. Further, whole-cell patch-clamp recordings confirm neurons behave rhythmically as they do in acute slice preparations. This work thus affirms that organotypic cultures retain the preBötC oscillator and can be used to probe the cellular and subcellular mechanisms of rhythmogenesis.

Chapter 2 further elaborates the organotypic slice culture model of respiration and leverages its optical qualities by investigating the electroresponsive properties of neurons generating rhythm in cultures. Two behaviorally distinct classes of rhythmic neurons known to exist in acute slices are also found to persist in cultures, which bolsters our confidence in the culture model of breathing behavior. One of these neuron types is hypothesized to be rhythmogenic, the other is thought to be

premotor-related. The subcellular distribution of a transient outward potassium current ( $I_A$ ) is one hallmark feature of the putatively rhythmogenic neuron type and its role dendritic responsive properties is examined in both rhythmic subtypes. The results demonstrate that rhythmically active neurons featuring  $I_A$  express it throughout the extent of their somatodendritic morphology. The subcellular distribution of  $I_A$  alters the electrotonic compactness of neurons and could support the notion that rhythmic neurons featuring  $I_A$  are most important for coordinating the onset of inspiratory burst activity.

This dissertation aims to demonstrate how current experimental obstacles in the study of respiratory rhythmogenesis can be overcome by the use of an alternative *in vitro* model of the behavior—the organotypic slice culture containing the preBötzinger complex. Although farther removed from the *in vivo* state than other acute preparations, this culture model appears to retain the core mechanisms necessary for stable rhythmogenesis. Improved optical qualities of organotypic cultures permit detailed imaging of dendritic processes and are leveraged to demonstrate unique integrative properties in rhythmically active respiratory neurons.

## REFERENCES

- Arsenault, J., Nagy, A., Henderson, J.T., and O'Brien, J.A. (2014). Regioselective Biolistic Targeting in Organotypic Brain Slices Using a Modified Gene Gun. *J. Vis. Exp. JoVE*.
- Beltran-Parrazal, L., Fernandez-Ruiz, J., Toledo, R., Manzo, J., and Morgado-Valle, C. (2012). Inhibition of endoplasmic reticulum Ca<sup>2+</sup> ATPase in preBötzinger complex of neonatal rat does not affect respiratory rhythm generation. *Neuroscience* 224, 116–124.
- Bittner, K.C., Grienberger, C., Vaidya, S.P., Milstein, A.D., Macklin, J.J., Suh, J., Tonegawa, S., and Magee, J.C. (2015). Conjunctive input processing drives feature selectivity in hippocampal CA1 neurons. *Nat. Neurosci.* 18, 1133–1142.
- Bouvier, J., Thoby-Brisson, M., Renier, N., Dubreuil, V., Ericson, J., Champagnat, J., Pierani, A., Chédotal, A., and Fortin, G. (2010). Hindbrain interneurons and axon guidance signaling critical for breathing. *Nat. Neurosci.* 13, 1066–1074.
- Czarnecki, A., Magloire, V., and Streit, J. (2008). Local oscillations of spiking activity in organotypic spinal cord slice cultures. *Eur. J. Neurosci.* 27, 2076–2088.
- Darbon, P., Tschertter, A., Yvon, C., and Streit, J. (2003). Role of the Electrogenic Na/K Pump in Disinhibition-Induced Bursting in Cultured Spinal Networks. *J. Neurophysiol.* 90, 3119–3129.
- Del Negro, C.A., Morgado-Valle, C., and Feldman, J.L. (2002). Respiratory Rhythm: An Emergent Network Property? *Neuron* 34, 821–830.
- Del Negro, C.A., Hayes, J.A., and Rekling, J.C. (2011). Dendritic Calcium Activity Precedes Inspiratory Bursts in preBötzinger Complex Neurons. *J. Neurosci.* 31, 1017–1022.
- Dong, H.-W., and Buonomano, D.V. (2005). A technique for repeated recordings in cortical organotypic slices. *J. Neurosci. Methods* 146, 69–75.
- Eldridge, F.L., Gill-Kumar, P., and Millhorn, D.E. (1976). Central neural stimulation of respiration in unanesthetized decerebrate cats. *J. Appl. Physiol.* 40, 23–28.

- Eldridge, F.L., Gill-Kumar, P., and Millhorn, D.E. (1981). Input-output relationships of central neural circuits involved in respiration in cats. *J. Physiol.* *311*, 81–95.
- Feldman, J.L., Del Negro, C.A., and Gray, P.A. (2013). Understanding the rhythm of breathing: so near, yet so far. *Annu. Rev. Physiol.* *75*, 423–452.
- Forsberg, D., Horn, Z., Tserga, E., Smedler, E., Silberberg, G., Shvarev, Y., Kaila, K., Uhlén, P., and Herlenius, E. (2016). CO<sub>2</sub>-evoked release of PGE<sub>2</sub> modulates sighs and inspiration as demonstrated in brainstem organotypic culture. *eLife* *5*, e14170.
- Foutz, A.S., Champagnat, J., and Denavit-Saubié, M. (1989). Involvement of N-methyl-d-aspartate (NMDA) receptors in respiratory rhythmogenesis. *Brain Res.* *500*, 199–208.
- Funk, G.D., and Greer, J.J. (2013). The rhythmic, transverse medullary slice preparation in respiratory neurobiology: Contributions and caveats. *Respir. Physiol. Neurobiol.* *186*, 236–253.
- Gähwiler, B.H. (1981). Morphological differentiation of nerve cells in thin organotypic cultures derived from rat hippocampus and cerebellum. *Proc. R. Soc. Lond. B Biol. Sci.* *211*, 287–290.
- Gähwiler, B.H. (1988). Organotypic cultures of neural tissue. *Trends Neurosci.* *11*, 484–489.
- Gidon, A., and Segev, I. (2012). Principles Governing the Operation of Synaptic Inhibition in Dendrites. *Neuron* *75*, 330–341.
- Gray, P.A., Rekling, J.C., Bocchiaro, C.M., and Feldman, J.L. (1999). Modulation of Respiratory Frequency by Peptidergic Input to Rhythmogenic Neurons in the PreBötzing Complex. *Science* *286*, 1566–1568.
- Guy, Y., Rupert, A., Sandberg, M., and Weber, S.G. (2011). A Simple Method for Measuring Organotypic Tissue Slice Culture Thickness. *J. Neurosci. Methods* *199*, 78–81.
- Humpel, C. (2015). Organotypic brain slice cultures: A review. *Neuroscience* *305*, 86–98.
- Jahnsen, H., Kristensen, B.W., Thiébaud, P., Noraberg, J., Jakobsen, B., Bove, M., Martinoia, S., Koudelka-Hep, M., Grattarola, M., and Zimmer, J.

- (1999). Coupling of Organotypic Brain Slice Cultures to Silicon-Based Arrays of Electrodes. *Methods* 18, 160–172.
- Kampa, B.M., and Stuart, G.J. (2006). Calcium Spikes in Basal Dendrites of Layer 5 Pyramidal Neurons during Action Potential Bursts. *J. Neurosci.* 26, 7424–7432.
- Laake, J.H., Haug, F.-M., Wieloch, T., and Ottersen, O.P. (1999). A simple in vitro model of ischemia based on hippocampal slice cultures and propidium iodide fluorescence. *Brain Res. Protoc.* 4, 173–184.
- Larkum, M.E., Zhu, J.J., and Sakmann, B. (1999). A new cellular mechanism for coupling inputs arriving at different cortical layers. *Nature* 398, 338–341.
- Larkum, M.E., Zhu, J.J., and Sakmann, B. (2001). Dendritic mechanisms underlying the coupling of the dendritic with the axonal action potential initiation zone of adult rat layer 5 pyramidal neurons. *J. Physiol.* 533, 447–466.
- Magee, J.C. (2000). Dendritic integration of excitatory synaptic input. *Nat. Rev. Neurosci.* 1, 181–190.
- Magloire, V., and Streit, J. (2009). Intrinsic activity and positive feedback in motor circuits in organotypic spinal cord slice cultures. *Eur. J. Neurosci.* 30, 1487–1497.
- Morgado-Valle, C., Beltran-Parrazal, L., DiFranco, M., Vergara, J.L., and Feldman, J.L. (2008). Somatic Ca<sup>2+</sup> transients do not contribute to inspiratory drive in preBötzinger Complex neurons. *J. Physiol.* 586, 4531–4540.
- Muller, D., Buchs, P.-A., and Stoppini, L. (1993). Time course of synaptic development in hippocampal organotypic cultures. *Dev. Brain Res.* 71, 93–100.
- Murphy, R.C., and Messer, A. (2001). Gene Transfer Methods for CNS Organotypic Cultures: A Comparison of Three Nonviral Methods. *Mol. Ther.* 3, 113–121.
- Newell, D.W., Barth, A., Papermaster, V., and Malouf, A.T. (1995). Glutamate and non-glutamate receptor mediated toxicity caused by oxygen and glucose deprivation in organotypic hippocampal cultures. *J. Neurosci.* 15, 7702–7711.

- Nguyen, T.D., Wirblich, C., Aizenman, E., Schnell, M.J., Strick, P.L., and Kandler, K. (2012). Targeted single-neuron infection with rabies virus for transneuronal multisynaptic tracing. *J. Neurosci. Methods* 209, 367–370.
- Otsu, Y., Marcaggi, P., Feltz, A., Isope, P., Kollo, M., Nusser, Z., Mathieu, B., Kano, M., Tsujita, M., Sakimura, K., et al. (2014). Activity-dependent gating of calcium spikes by A-type K<sup>+</sup> channels controls climbing fiber signaling in Purkinje cell dendrites. *Neuron* 84, 137–151.
- Pace, R.W., and Del Negro, C.A. (2008). AMPA and metabotropic glutamate receptors cooperatively generate inspiratory-like depolarization in mouse respiratory neurons in vitro. *Eur. J. Neurosci.* 28, 2434–2442.
- Pace, R.W., Mackay, D.D., Feldman, J.L., and Del Negro, C.A. (2007a). Inspiratory bursts in the preBötzing complex depend on a calcium-activated non-specific cation current linked to glutamate receptors in neonatal mice. *J. Physiol.* 582, 113–125.
- Pace, R.W., Mackay, D.D., Feldman, J.L., and Del Negro, C.A. (2007b). Role of persistent sodium current in mouse preBötzing Complex neurons and respiratory rhythm generation. *J. Physiol.* 580, 485–496.
- Peña, F. (2010). Organotypic cultures as tool to test long-term effects of chemicals on the nervous system. *Curr. Med. Chem.* 17, 987–1001.
- Picardo, M.C.D., Weragalaarachchi, K.T.H., Akins, V.T., and Del Negro, C.A. (2013). Physiological and morphological properties of Dbx1-derived respiratory neurons in the pre-Bötzing complex of neonatal mice. *J. Physiol.* 591, 2687–2703.
- Pierrefiche, O., Foutz, A.S., Champagnat, J., and Denavit-Saubié, M. (1994). NMDA and non-NMDA receptors may play distinct roles in timing mechanisms and transmission in the feline respiratory network. *J. Physiol.* 474, 509–523.
- Poirazi, P., Brannon, T., and Mel, B.W. (2003). Pyramidal Neuron as Two-Layer Neural Network. *Neuron* 37, 989–999.
- Ramirez, J.M., Schwarzacher, S.W., Pierrefiche, O., Olivera, B.M., and Richter, D.W. (1998). Selective lesioning of the cat pre-Bötzing complex in vivo eliminates breathing but not gasping. *J. Physiol.* 507, 895–907.

- Rathenberg, J., Nevian, T., and Witzemann, V. (2003). High-efficiency transfection of individual neurons using modified electrophysiology techniques. *J. Neurosci. Methods* 126, 91–98.
- Rekling, J.C., Champagnat, J., and Denavit-Saubie, M. (1996). Electroresponsive properties and membrane potential trajectories of three types of inspiratory neurons in the newborn mouse brain stem in vitro. *J. Neurophysiol.* 75, 795–810.
- Richter, D.W. (1982). Generation and maintenance of the respiratory rhythm. *J. Exp. Biol.* 100, 93–107.
- Ruangkittisakul, A., Schwarzacher, S.W., Secchia, L., Poon, B.Y., Ma, Y., Funk, G.D., and Ballanyi, K. (2006). High Sensitivity to Neuromodulator-Activated Signaling Pathways at Physiological [K<sup>+</sup>] of Confocally Imaged Respiratory Center Neurons in On-Line-Calibrated Newborn Rat Brainstem Slices. *J. Neurosci.* 26, 11870–11880.
- Ruangkittisakul, A., Panaitescu, B., and Ballanyi, K. (2011). K<sup>+</sup> and Ca<sup>2+</sup> dependence of inspiratory-related rhythm in novel “calibrated” mouse brainstem slices. *Respir. Physiol. Neurobiol.* 175, 37–48.
- Ruangkittisakul, A., Kottick, A., Picardo, M.C.D., Ballanyi, K., and Del Negro, C.A. (2014). Identification of the pre-Bötzinger complex inspiratory center in calibrated “sandwich” slices from newborn mice with fluorescent Dbx1 interneurons. *Physiol. Rep.* 2.
- Rytter, A., Cronberg, T., Asztély, F., Nemali, S., and Wieloch, T. (2003). Mouse Hippocampal Organotypic Tissue Cultures Exposed to In Vitro “Ischemia” Show Selective and Delayed CA1 Damage that is Aggravated by Glucose. *J. Cereb. Blood Flow Metab.* 23, 23–33.
- Schwarzacher, S.W., Smith, J.C., and Richter, D.W. (1995). Pre-Botzinger complex in the cat. *J. Neurophysiol.* 73, 1452–1461.
- Seidl, A.H., and Rubel, E.W. (2010). A Simple Method for Multi-Day Imaging of Slice Cultures. *Microsc. Res. Tech.* 73, 37–44.
- Smith, J.C., and Feldman, J.L. (1987). In vitro brainstem-spinal cord preparations for study of motor systems for mammalian respiration and locomotion. *J. Neurosci. Methods* 21, 321–333.

- Smith, J.C., Morrison, D.E., Ellenberger, H.H., Otto, M.R., and Feldman, J.L. (1989). Brainstem projections to the major respiratory neuron populations in the medulla of the cat. *J. Comp. Neurol.* *281*, 69–96.
- Smith, J.C., Greer, J.J., Liu, G.S., and Feldman, J.L. (1990). Neural mechanisms generating respiratory pattern in mammalian brain stem-spinal cord in vitro. I. Spatiotemporal patterns of motor and medullary neuron activity. *J. Neurophysiol.* *64*, 1149–1169.
- Smith, J.C., Ellenberger, H.H., Ballanyi, K., Richter, D.W., and Feldman, J.L. (1991). Pre-Bötzinger Complex: A Brainstem Region That May Generate Respiratory Rhythm in Mammals. *Science* *254*, 726–729.
- Stoppini, L., Buchs, P.-A., and Muller, D. (1991). A simple method for organotypic cultures of nervous tissue. *J. Neurosci. Methods* *37*, 173–182.
- Stoppini, L., Buchs, P.-A., and Muller, D. (1993). Lesion-induced neurite sprouting and synapse formation in hippocampal organotypic cultures. *Neuroscience* *57*, 985–994.
- Stuart, G.J., and Spruston, N. (2015). Dendritic integration: 60 years of progress. *Nat. Neurosci.* *18*, 1713–1721.
- Stuart, G.J., Häusser, Michael, and Spruston, N. (2016). *Dendrites* (Oxford, UK: Oxford University Press).
- Suzue, T. (1984). Respiratory rhythm generation in the in vitro brain stem-spinal cord preparation of the neonatal rat. *J. Physiol.* *354*, 173–183.
- Tscherter, A., Heuschkel, M.O., Renaud, P., and Streit, J. (2001). Spatiotemporal characterization of rhythmic activity in rat spinal cord slice cultures. *Eur. J. Neurosci.* *14*, 179–190.
- Wickersham, I.R., Lyon, D.C., Barnard, R.J.O., Mori, T., Finke, S., Conzelmann, K.-K., Young, J.A.T., and Callaway, E.M. (2007). Monosynaptic Restriction of Transsynaptic Tracing from Single, Genetically Targeted Neurons. *Neuron* *53*, 639–647.
- Yamamoto, N., Higashi, S., and Toyama, K. (1997). Stop and Branch Behaviors of Geniculocortical Axons: A Time-Lapse Study in Organotypic Cocultures. *J. Neurosci.* *17*, 3653–3663.

- Zhabotinski, Y.M., Chumasov, E.I., Chubakov, A.R., and Konovalov, H.V. (1979). Development of synaptic structure and function in organotypic cultures of the rat hippocampus. *Neuroscience* 4, 913–920.
- Zimmer, J., and Gähwiler, B.H. (1987). Growth of hippocampal mossy fibers: A lesion and coculture study of organotypic slice cultures. *J. Comp. Neurol.* 264, 1–13.

## **CHAPTER 1: Organotypic slice cultures containing the preBötzinger complex generate respiratory-like rhythms**

### **1.1 INTRODUCTION**

For nearly twenty-five years, investigators have employed acute transverse slice preparations containing the preBötzinger complex (preBötC) to probe the cellular and synaptic bases for respiratory rhythm generation in rodents (Feldman et al., 2013; Funk and Greer, 2013; Smith et al., 1991). These ‘breathing slice’ preparations retain sufficient circuitry from the respiratory medulla to spontaneously generate inspiratory-related rhythms and motor output, measurable via the hypoglossal (XII) cranial nerve root. Acute slices provide optimal access for electrophysiological, optical, and pharmacological experiments, which has helped define fundamental cellular and synaptic neural mechanisms underlying inspiratory rhythms as well as basic neuromodulatory mechanisms that influence network activity (Feldman et al., 2013; Funk and Greer, 2013; Ramirez et al., 2012).

However, acute slices remain viable and rhythmically active for approximately one day (Funk and Greer, 2013), which limits the scope of techniques that may be applied. Pharmacological assays are limited to time windows of several hours,

which prohibit studies of chronic drug effects on respiratory network function. Furthermore, experiments that involve genetic manipulation or transfection require several days for protein expression, and thus are impossible using acute slices. It would therefore be advantageous to have an in vitro preparation that retains a functional preBötC for days or weeks, and facilitates genetic and pharmacological manipulation while retaining behaviorally relevant network activity that can be monitored and recorded with the ease offered by acute slices.

Using organotypic culturing techniques, partial slice preparations of the preBötC have been successfully maintained over multi-week periods (Hartelt et al., 2008). These slice cultures, cut 250  $\mu\text{m}$  thick, preserve some rhythmogenic function, but contain only a fraction of the preBötC neurons normally captured in 400-700  $\mu\text{m}$  thick breathing slices (Funk and Greer, 2013). Hartelt and colleagues recorded rhythmic low-frequency action potential bursts in some cells, but did not analyze whether coordinated patterns of network activity were generated in their cultures. Thus, a culture preparation that retains the preBötC rhythmogenic core bilaterally, throughout its anterior-posterior extent, which typifies acute rhythmically active slice preparations, has not yet been described.

Here we present a novel slice preparation that retains the preBötC bilaterally using both the Stoppini membrane method and Gähwiler roller-drum method of organotypic slice culturing (Gähwiler, 1981; Stoppini et al., 1991). This new culture preparation generates synchronized network activity bilaterally in the ventrolateral, preBötC-related regions of the slice, analogous to rhythms in acute slice preparations. The preparation shows spontaneous rhythm over several weeks of

culturing, and flattens out, which improves the quality of optical imaging at the cellular and network level. Furthermore, the neurons are accessible for whole-cell patch clamping, meaning that both network activity and individual neurons can be selectively recorded from and perturbed using methods already established in the acute slice preparation.

## 1.2 RESULTS

### **Oscillatory activity in acute slices, brainstem slice cultures, and brainstem-cerebellar co-cultures**

Bilateral oscillatory calcium activity was detected in Fluo-8 AM-loaded brainstem slices that expose the preBötC at their rostral surface (Ruangkittisakul et al., 2011, 2014), and subsequently imaged both acutely, and after 7-28 days DIV using the Stoppini culturing method (Fig. 1.1A,B). In both acute slices and cultures synchronized calcium activity was observed in an inverted V-shaped pattern with signals concentrated in dorsal (Fig. 1.1A,B, blue circles) and ventral (Fig. 1.1A,B, red circle) oscillatory groups. Acute slices showed respiratory-related rhythmic activity at  $10.9 \pm 4.2$  bursts/min ( $n = 10$ ) and slices maintained in organotypic culture for 7-22 DIV oscillated at  $13.7 \pm 10.6$  ( $n = 15$ ) bursts/min. When we co-cultured the brainstem slice with two cerebellar slice explants (placed either along the dorsolateral or ventrolateral border of the slice) then the rhythm was faster ( $22.4 \pm 8.3$  bursts/min,  $n = 26$ , Fig. 1.1C,D). Brainstem-cerebellar co-cultures (7-43 DIV) were faster than both acute slices and brainstem slice cultures, and there was no significant linear correlation, or other obvious relationship between DIV and burst frequency (not shown, linear correlation coefficient  $r = 0.1$ ,  $n = 19$ ).

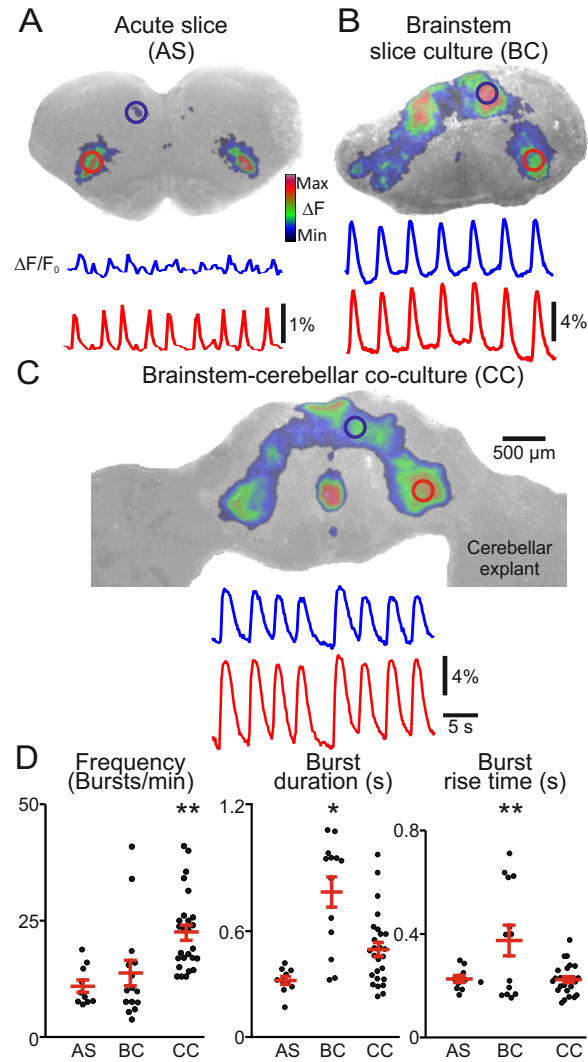


**Figure 1. 1** Oscillatory calcium activity in three different transverse brainstem slice preparations. **A**, *top panel*: Cycle-triggered average of fluorescent calcium activity overlaid on brightfield image of an acute slice preparation (AS, for anatomical reference). ROIs drawn over rhythmically active areas at ventrolateral (red) and dorsomedial regions (blue). *Bottom panel*:  $\Delta F/F_0$  traces of rhythmic activity. Upper/blue trace corresponds to dorsomedial ROI; lower/red trace corresponds to ventrolateral ROI. **B,C**: Same as in **A**, showing calcium activity from a brainstem slice culture (BS), and a brainstem-cerebellar co-culture preparation (CC), respectively. The color calibration scale in **A** shows the colors associated with the  $\Delta F$  range from minimal to maximal, and applies to all plots in figures showing  $\Delta F$  images. **D**: Graphs showing burst frequency, burst duration (half-width; taken at 50% from baseline), and burst rise-time (10-90% amplitude from baseline). Error bars: Means  $\pm$  SEM. \*P < 0.05, \*\*P < 0.001, ANOVA with post hoc comparison using Tukey tests. Note that the burst frequency is higher in co-culture preparations versus acute slice and brainstem slice cultures. Also, the difference in burst duration and rise time between acute slice and co-culture preparations is not significant.

Preparation type had a significant effect on frequency ( $F[2,48] = 8.9$ ,  $p = 0.0005$ , Fig. 1.1D, left panel). Post hoc comparison using Bonferroni or Tukey tests indicate that co-culture oscillation frequency is significantly different than brainstem slice cultures (mean difference = 8.7 bursts/min,  $p = 0.008$ ) and acute slices (mean difference = 11.5 bursts/min,  $p = 0.002$ ).

Calcium transients in brainstem slice cultures were longer lasting and had a slower onset compared to acute slices or brainstem-cerebellar co-cultures. The mean burst duration of calcium activity in the ventral oscillatory group of brainstem slice cultures measured  $785 \pm 257$  ms ( $n=13$ ) compared to  $367 \pm 59$  ms in acute slice preparations ( $n = 10$ ) and  $514 \pm 169$  ms in co-cultures ( $n = 26$ ). Preparation type had a significant effect on burst duration ( $F[2,46] = 16.2$ ,  $p = 4.7 \times 10^{-6}$ , Fig. 1.1D, center panel). Post hoc comparison tests indicate that brainstem slice culture burst duration is significantly different than both acute slices (mean difference = 418 ms,  $p=6.1 \times 10^{-6}$ ) and co-cultures (mean difference = 272 ms,  $p=0.0002$ ).

The rate of signal onset, measured as the 10-90% rise-time above baseline fluorescence, was slower in brainstem slice cultures ( $375 \pm 213$  ms,  $n = 13$ ) compared to acute slice preparations ( $226 \pm 43$  ms,  $n = 10$ ) and co-cultures ( $223 \pm 57$  ms,  $n = 26$ ). Preparation type had a significant effect on signal onset ( $F[2,46]=7.8$ ,  $p=0.001$ , Fig. 1.1D, right panel) and post hoc comparison tests indicate that burst rise-time brainstem slice culture is significantly different than both acute slices (mean difference = 149 ms,  $p=0.01$ ) and co-cultures (mean difference = 152 ms,  $p = 0.001$ ).

The signal-to-noise ratio was higher in co-cultured preparations compared to acute slices. Under similar dye-loading and imaging conditions, peak calcium signals from the center of the ventral oscillatory group measured 340% higher in magnitude in co-cultured preparations ( $5.5 \pm 3.3$  %,  $n = 8$ ), and 550% higher in brainstem slice culture preparations ( $8.8 \pm 3.1$  %,  $n = 8$ ) compared to acute preparations ( $1.6 \pm 0.7$  %,  $n = 8$ , ( $F[2,21] = 14.8$ ,  $p = 9.6E-5$ ). Active areas whose calcium activity was not normally visible in acute slices also became apparent in cultured preparations. In 53% ( $n = 34$ ) of all cultured preparations, midline activity between ventral oscillatory groups was detectable.

We also prepared brainstem slices co-cultured with cerebellar explants using Roller-drum methods (Gahwiler, 1981), and these cultures (17-19 DIV) also showed spontaneous oscillatory activity, with a burst frequency of  $28.6 \pm 5.9$  bursts/min, burst duration of  $625 \pm 97$  ms, and 10-90% rise-time of  $269 \pm 29$  ms. These characteristic measurements were not significantly different from similar Stoppini-type co-cultures ( $p = 0.09-0.16$ ,  $n=5$ ).

### **Spread of activity in brainstem slice cultures and brainstem-cerebellar co-cultures**

Both brainstem slice cultures and brainstem-cerebellar co-cultures display oscillatory calcium burst patterns that propagate ipsilaterally, travelling from their point of initiation in the ventrolateral area toward the dorsomedial border at varying velocities (Fig. 1.2A). When imaged at 129 Hz, the signal in brainstem-cerebellar co-cultures propagated 275 % as fast ( $0.022 \pm 0.007$  m/s,  $n = 8$ ) as brainstem slice cultures ( $0.008 \pm 0.005$  m/s,  $n = 9$ ,  $p < 0.001$ ; Fig. 1.2B). In each slice there was a

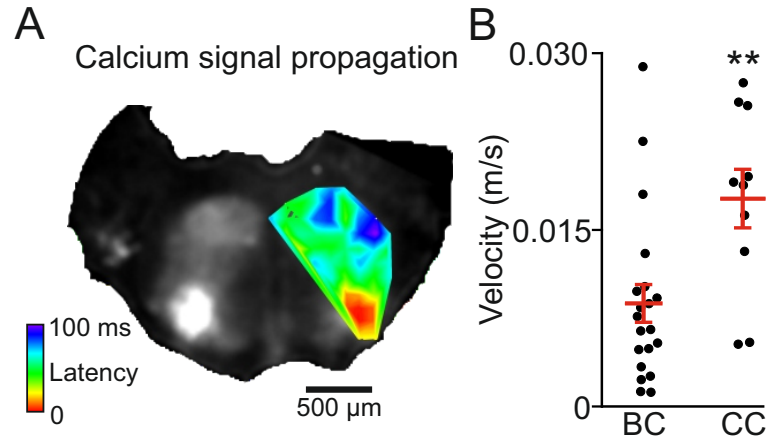


**Figure 1. 2** Propagation of calcium activity in brainstem slice cultures and brainstem-cerebellar co-cultures. **A:** Time series Z-projection of maximum fluorescent calcium activity in a brainstem-cerebellar co-culture. The heat map overlay shows threshold signal increases from low (red) to high latencies (blue) during a single rhythmic burst acquired at 129 frames/s. **B:** Average velocity of signal propagation in brainstem slice cultures (BC) versus brainstem-cerebellar co-cultures (CC). Error bars: Means  $\pm$  SEM. \*\* $P < 0.001$ , Student's t-test.

detectable latency in the signal rise between contralateral ventral oscillatory groups. In every case, for both brainstem slice cultures and brainstem-cerebellar co-cultures, calcium signals took longer to propagate from ventral to dorsal regions than to contralaterally equivalent regions, where the activity appeared within 1-2 frames, which made it too uncertain to calculate a precise velocity or possible dominant or alternating initiation site ( $n = 7$ ). Thus, regardless of preparation type, synchronized bursts first occurred bilaterally between contralateral ventral oscillatory groups and then propagated more slowly in the dorsomedial direction.

### **Ventral oscillatory group activity in multiple neurons and calcium transients in dendritic profiles**

In acute slice preparations, calcium and voltage dye fluorescence imaging often appears as diffuse regional fluorescence due to light scattering in the tissue, or instead captures only a subset of rhythmically active neurons within the field of

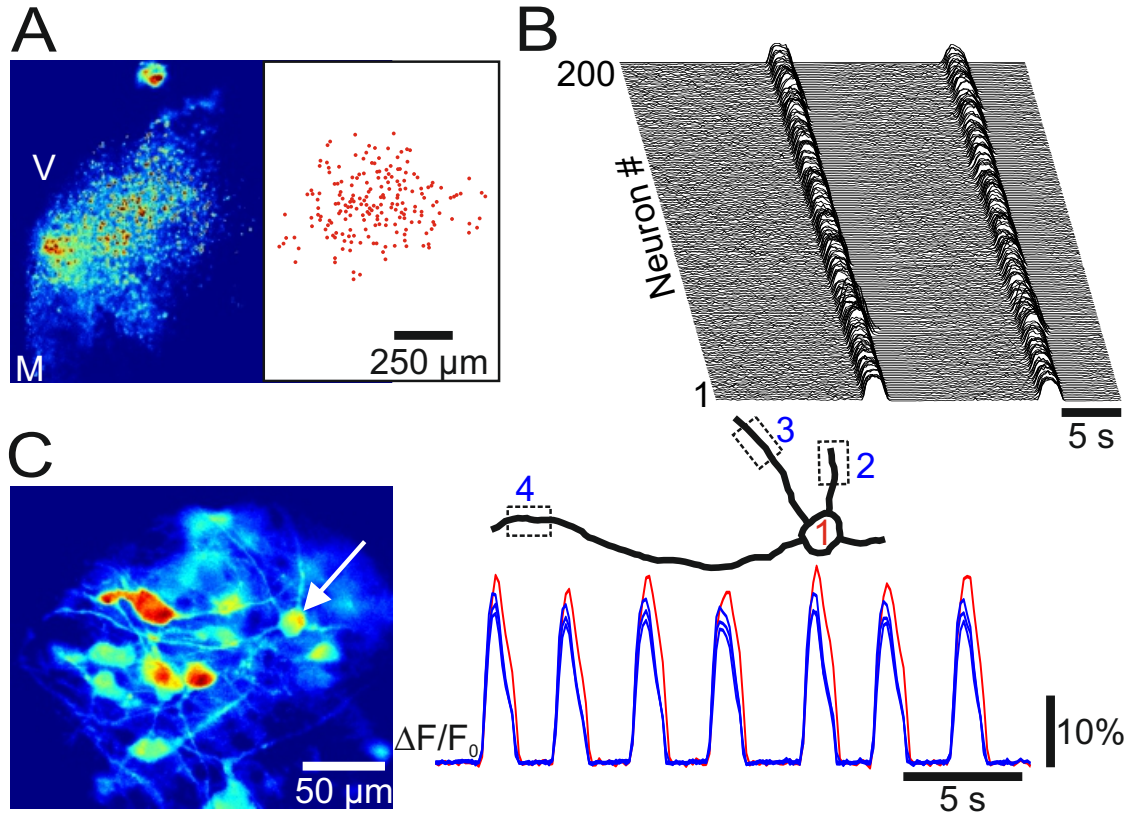


**Figure 1.3** Low and high magnification views of oscillatory activity. **A:** Left panel, oscillatory calcium activity in the ventral oscillatory group at low magnification using 10x objective (Z-projection of STANDARD DEVIATION from 200 frame image stack at 10 Hz, V: Ventral, M: Medial). Right panel, position of 200 oscillating cell body ROIs from the image in **A**. **B:** Waterfall diagram of  $\Delta F/F_0$  traces from the 200 ROIs shown in **A**. Note the tight synchronization during two cycles. **C:** Left panel, cycle-triggered average of oscillatory calcium activity at high magnification using a 63x objective. Note the visualization of somas and dendritic profiles. Right panel, reconstruction of the soma-dendritic territory from one neuron, and the associated  $\Delta F/F_0$  traces from three dendritic and one somatic ROI (indicated by dotted squares).

scattering at locations deep within the slice (Del Negro et al., 2011; Funk and Greer, 2013; Katona et al., 2011). One advantage of culturing brain slices is the reduced thickness compared to acute slices (Stoppini et al., 1991). Using the Stoppini culturing method, we reduced the thickness of the brainstem slices cultured here to  $104 \pm 31 \mu\text{m}$  (measured in sagittal sections of Epon-embedded 7-31 DIV oscillating cultures,  $n = 5$ ) from a thickness of  $400 \mu\text{m}$  in the acute slices at

0 DIV. The dorsal-to-ventral distance at the slice midline increased to  $1943 \pm 183$   $\mu\text{m}$  compared to  $1490 \pm 74$   $\mu\text{m}$  in acute slices acquired from age-matched controls (P2.5,  $p < 0.05$ ,  $n = 5$ ). Thus, the cultures flatten out and the reduced thickness made it possible to record synchronized calcium transients from hundreds of neurons in the same focal plane (Fig. 1.3A,B). At higher magnification both somatic and proximal ( $\sim 100$   $\mu\text{m}$ ) dendritic activity could be recorded in Fluo-8 AM-loaded neurons (Fig. 1.3C).

### **Retrograde biocytin labeling in Roller-drum cultures**

The preBötC contains commissural interneurons, which synchronize bilateral halves of the preBötC, as well as interneurons that project ipsilaterally to premotor neurons in the intermediate reticular formation, as well as hypoglossal motor neuron pools (Wang et al., 2014). If the inverted V-shaped pattern of rhythmic calcium activity in cultures corresponds to that seen in acute slices, then similar axon projections ought to be maintained in the cultured preparation. To test this prediction, we electroporated 1% biocytin using patch pipettes placed in the ventral oscillatory group of Roller-drum cultures ( $n = 3$ ). Retrogradely labeled neurons were located around the injection site, somatas and projecting fibres were found in the ipsilateral dorsal part the culture, the midline, and in the contralateral ventrolateral part of the cultures (Fig. 1.4B,C). The somatic positions of the labeled neurons and fibres corresponded to oscillatory regions recorded before electroporation (Fig. 1.4A,B). . The biocytin labeling suggests that the pattern of activity in cultures is attributable to an underlying bilateral network of neurons in

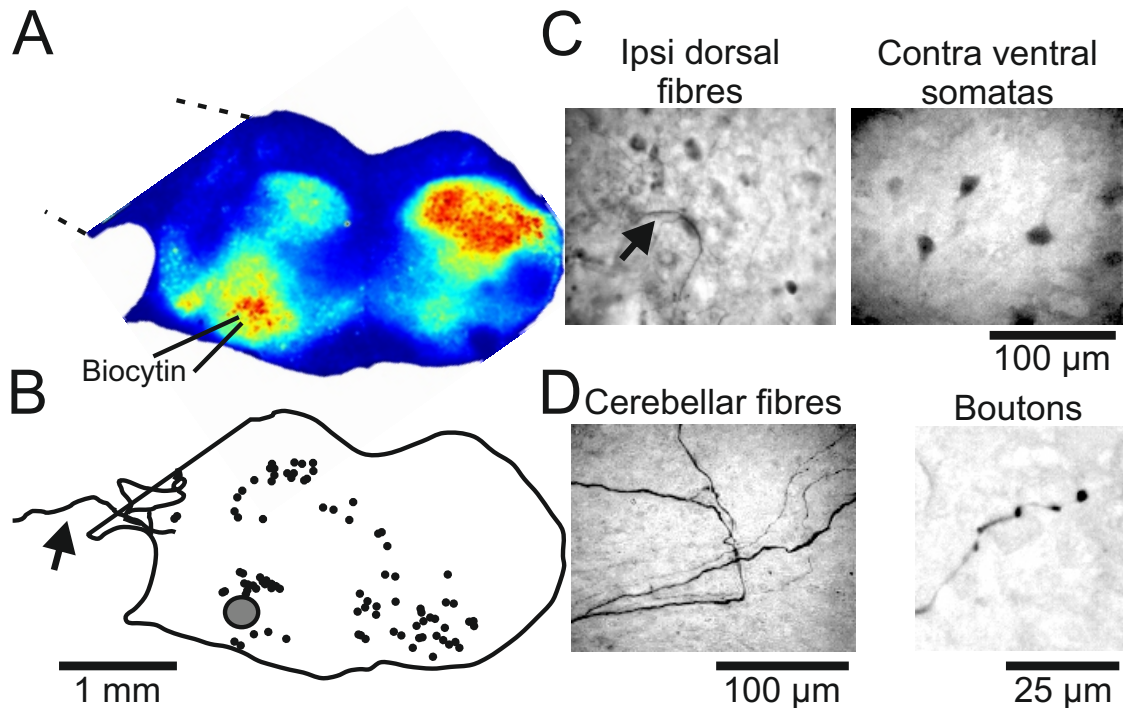


**Figure 1.4** Retrograde labeling of neurons following local co-iontophoresis of biocytin and KCl in roller-drum cultures. **A:** Oscillatory calcium activity (Z-projection of STANDARD DEVIATION from 300 frame image stack) in a Roller-drum brainstem-cerebellar co-culture. **B:** Camera-lucida reconstruction of the position of retrogradely labeled neurons (filled circles) after local co-iontophoresis at the ventral oscillatory group (gray circle). Note that some labeled fibers cross into the cerebellar explant (arrow). **C:** Photomicrograph of labeled fibres located in the ipsilateral dorsal, and somatas in the contralateral ventral part of the co-culture. **D:** Photomicrograph of labeled fibres entering the cerebellar part of the cultures, and ending in boutons.

structures were detected in one slice co-culture (Fig. 1.4B,D), indicating a degree of synaptic interconnectivity between the brainstem and cerebellar neurons.

### Calcium activity in GFAP+ labeled cells

Oscillatory calcium transients have been reported in astrocytes in sync with neighboring preBötC neurons (Oku et al., 2015). We tested for rhythmic glial activity in brainstem-cerebellar co-cultures prepared from transgenic mice that express EGFP coupled to glial fibrillary acidic protein (Fig. 1.5). However, oscillatory calcium fluorescence was undetectable in 98% (n = 288, 10 cultures) of

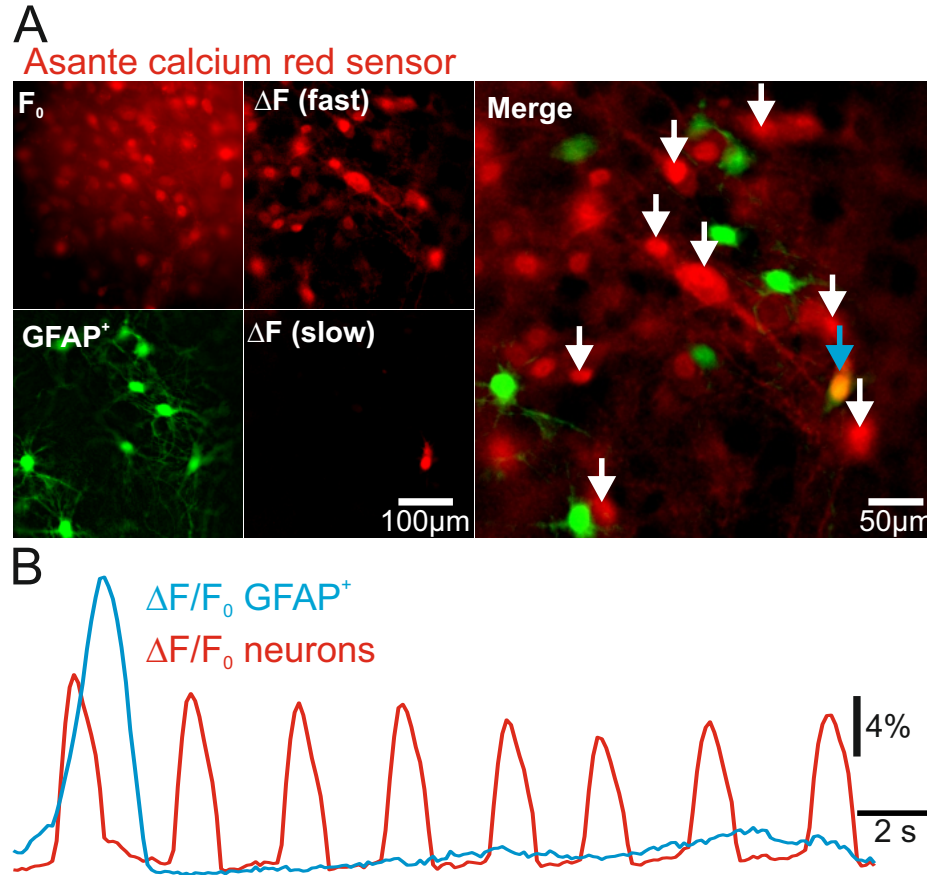


**Figure 1. 5** Simultaneous imaging of GFAP<sup>+</sup> cells expressing EGFP (green channel) and time-series of fluorescent calcium activity (red channel). **A**, *Top-left quarter-panel*: Baseline calcium ( $F_0$ ) with a cycle-triggered average of calcium fluorescence taken between rhythmic events. *Bottom-left quarter-panel*: Expression of EGFP in GFAP<sup>+</sup> cells in the same field of view. *Top-right quarter-panel*: Cycle-triggered average of maximum calcium fluorescence during fast rhythmic burst events ( $\Delta F$  (fast)) minus baseline fluorescence. *Bottom-right quarter-panel*: Z-projection sum of  $\Delta F/F_0$  across  $t=0.7-3.2s$  showing a slow independent calcium transient ( $\Delta F$  (slow)). *Right*: Merge of EGFP expression, cycle-triggered average maxima, and the Z-projection sum of the slow calcium transient; overlap between green and red channels is shown at the blue arrow. **B**:  $\Delta F/F_0$  plot of rhythmic neuronal calcium activity (red) versus GFAP<sup>+</sup>-associated calcium activity (blue). Neuronal activity was averaged from 8 ROIs indicated by white arrows in center-panel of **A**. GFAP<sup>+</sup> ROI is indicated by blue arrow.

the recorded GFAP<sup>+</sup> cells (Fig. 1.5A). A few EGFP-expressing astrocytes ( $n = 5$ ) generated one-time calcium transients independently of calcium transients in neighboring oscillating neurons (Fig. 1.5B,  $n = 4$ ). The mean rise-time of these transient events ( $810 \pm 235$  ms,  $n = 5$ ) exceeded the length of calcium transients

in neighboring rhythmic neurons ( $393 \pm 66$  ms;  $n = 119$  neurons, across 5 cultures,  $p=0.0051$ ). Half-width duration of transients in GFAP-cells ( $1028 \pm 124$  ms) was 24% longer than rhythmic neurons ( $866 \pm 31$  ms;  $n = 119$  cells, across 5 cultures,  $p = 0.022$ ).

### **Whole-cell electrophysiology**

To assess whether neuronal behavior in cultures resembles preBötC neurons in acute slice preparations (Funk and Greer, 2013), we recorded the voltage trajectory in rhythmic neurons from culture preparations. First, using calcium imaging, rhythmically active cells within the ventral oscillatory group were targeted for whole-cell patch-clamp recordings (Fig. 1.6A,  $n = 10$ ). Rhythmic drive potentials ( $343 \pm 207$  ms duration,  $n = 7$ ) that reflect underlying network activity were recorded at typical membrane potential (overriding action potentials were removed via bandpass filtering), and at hyperpolarized potentials using negative bias current to uncover non-linear membrane behavior indicative of recruitment of active conductances (Fig. 1.6B). The amplitude of the underlying drive potential was 185% larger in rhythmic neurons held at close to resting membrane potential ( $19.0 \pm 6.6$  mV;  $n = 7$ ), than in neurons held at membrane potentials below the threshold of action potential generation during the burst ( $10.3 \pm 3.7$  mV;  $n = 5$ ,  $p < 0.05$ ).

Finally, we tested pharmacological modulation of burst frequency by neuropeptides. From a control frequency of  $24.4 \pm 6.4$  bursts/min, the NK1-receptor agonist Substance P (SP, 500 nM) sped up the frequency by 134% to  $32.7 \pm 9.3$  bursts/min ( $p < 0.05$ ), and adding the  $\mu$ -opioid agonist DAMGO (1  $\mu$ M)

on top of SP slowed the frequency by 50% to  $16.5 \pm 8.7$  bursts/min ( $p < 0.01$ ,  $n = 6$  cumulative dosings, Fig. 1.6C).

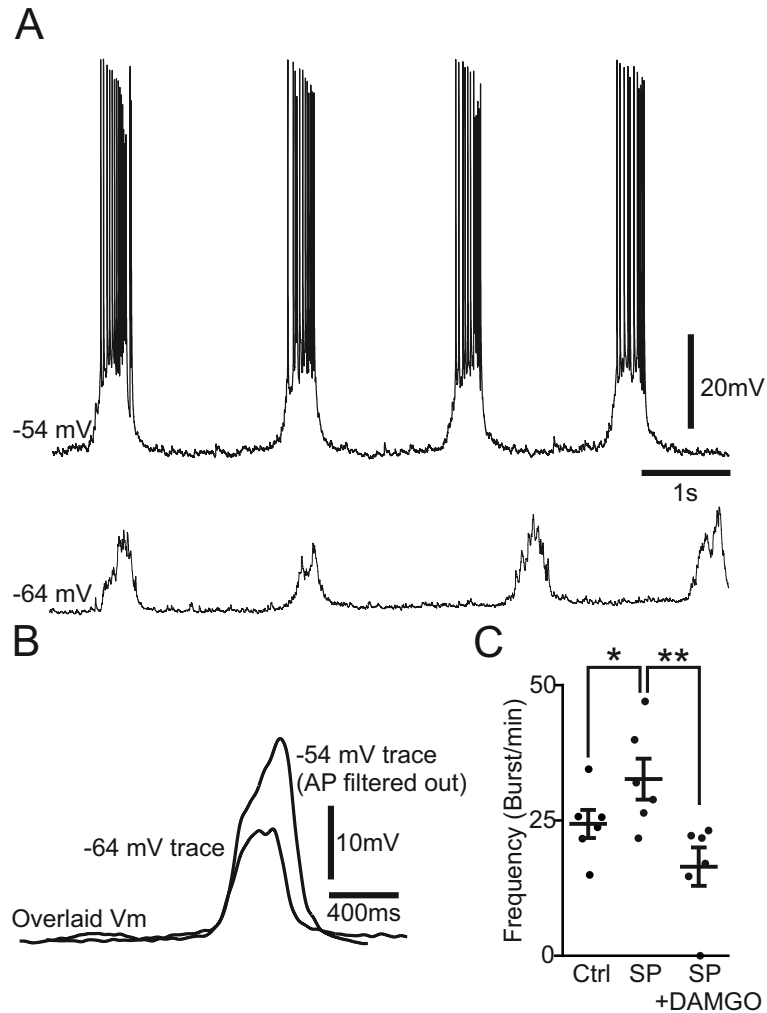


**Figure 1. 6** Whole-cell patch clamp recordings from a rhythmically active neuron in the ventral oscillatory group of a brainstem-cerebellar co-culture after 7 DIV. **A**, *Top trace*: normal bursting activity at resting Vm with zero current bias applied. *Bottom trace*, Rhythmic drive potential at a hyperpolarized potential, after negative bias (-0.1 nA) applied. **B**: Overlaid cycle-triggered, and action potential-filtered average traces of the burst events occurring in **A** and **B**. Note that the underlying burst envelope is larger in amplitude at resting Vm levels. **C**. Modulation of burst frequency by 500 nM Substance P (SP), and 500 nM SP + 1  $\mu$ M DAMGO. Error bars: Means  $\pm$  SEM. \* $p < 0.05$ , \*\* $p < 0.001$ ,  $n = 6$ , paired sample t-Test, control versus SP, and SP versus SP plus DAMGO.

### 1.3 DISCUSSION

Acute slice preparations containing the preBötC survive in organotypic culture conditions and maintain patterned rhythmic calcium activity, which we attribute to underlying neuronal inspiratory-like drive potentials and spike bursts in constituent preBötC interneurons. Bursts in culture begin with fast bilateral co-activation in ventrolateral regions of the slice and then propagate ipsilaterally to the dorsomedial regions of the culture preparations. The inverted V-shaped activity pattern was consistent; it did not depend on the presence of cerebellar explants. The ipsilateral ventral-to-dorsal propagation velocity was on the order of 0.02 m/s in brainstem-cerebellar slice cultures. This velocity is roughly 10 times slower than a published value of 0.24 m/s in the commissural fiber tracts connecting bilateral preBötC in rhythmically active acute slices of neonatal rats using voltage-imaging (Koshiya et al., 2014). Thus, the slice cultures appear to generate patterned activity that spreads dorsally slower than the normal velocity of fine axons abundant in the neonatal central nervous system (Sternberger et al., 1979), which may imply that the activity is shaped by local synaptic processes in networks of neurons. The pattern also overlaps the expression of cells—in the transverse plane of the brainstem and cervical spinal cord—derived from the homeodomain transcription factor, *Dbx1*, which gives rise to rhythmogenic interneurons that comprise the preBötC (Bouvier et al., 2010; Gray et al., 2010; Picardo et al., 2013) and also play a role in premotor drive transmission (Wang et al. 2014).

In some recordings we also observed midline activity, which may reflect raphe neurons that interconnect with the preBötC and increase firing frequency in

response to rhythmic preBötC input (Ptak et al., 2009). Retrograde biocytin labeling from the ventral oscillatory group reveals projections in both the contralateral ventral oscillatory group and dorsomedial regions, similar to that obtained via in vivo fluoro gold injection into the preBötC (Koshiya et al., 2014). Retrogradely labeled neurons were also found in the midline, further suggesting the involvement of raphe neurons. Thus it appears unlikely that rhythmic calcium changes in the slice occur due to spontaneous calcium oscillations, but rather they resemble the neuronal behavior found in acute slices, similar in both dynamics and patterning, and occurring over anatomical regions that correspond to known areas of activity, and to locations of cells vital for production of the respiratory rhythm. The presence of cerebellar explants co-cultured with preBötC slices bolsters the rhythm, causing it to oscillate faster than acute preBötC preparations, but with similar burst duration and 10-90% rise-times. Without the addition of cerebellar explants, brainstem cultures oscillate at the same frequency as acute preparations but individual bursts have a slower onset and offset—increased burst duration and rise time. Although the specific roles of cerebellar explants that promote preBötC-like rhythmic activity in cultures are unknown, spontaneous oscillatory activity in cerebellar granule cells may contribute to the overall excitability of the slice (Apuschkin et al., 2013; De Zeeuw et al., 2008), especially if co-culturing allows granule cell axon entry into the preBötC and facilitates excitatory synaptic connections with preBötC interneurons of the ventral oscillatory group. Since preBötC-like rhythmic behavior occurred in the absence of cerebellar explants, but that these rhythms were faster with cerebellar co-cultures, we conclude that

cerebellar circuits augment excitability in the cultured preBötC but do not contribute to the cellular mechanisms underlying rhythm generation.

Due to gradual thinning of the slice and consequent reduction of light scattering in the tissue over time, the brainstem slice culture preparation allows for higher spatial resolution when imaging at both the cellular and network level and greater amplitude of fluorescent signals. This could be advantageous for analyzing larger portions of rhythmically active cell populations in the preBötC and adjacent premotor areas than has previously been possible in acute slices. For example, the culture preparation we characterize here may facilitate real-time visualization and perturbation of individual burst percolation across the rhythmogenic core and into premotor areas. Our preparation makes it feasible to stimulate and record large populations (~100s of neurons), since neighboring somata that would otherwise be spread through the Z-axis become coplanar (or nearly so for practical purposes). These conditions also simplify imaging requirements: population-level recordings could be acquired using wide-field excitation. Additionally, subcellular sections of neurons (e.g. dendritic processes) can be visualized at higher magnifications. Therefore, it is more likely that several hundred micron regions of dendritic processes can be captured in a single focal plane, and thus intercellular signal propagation arising from recurrent excitation along the dendritic arborization of rhythmic neurons, and its impact on burst generation, might also be more readily visualized.

Astrocytes have been implicated in respiratory rhythm generation (Hartel et al., 2009; Hulsman et al., 2000; Oku et al., 2015; Schnell et al., 2011). We tested for

the presence of calcium oscillations in the astrocytes of brainstem-cerebellar co-cultures. We were able to image a large number of cells simultaneously using conventional wide-field illumination microscopy. We used a bath-applied red-shifted calcium indicator, despite an inherently reduced fluorescence intensity compared to brighter green dyes (e.g. OGB1, Fluo-8), because of the flattened state and reduced tortuosity in the culture preparation. There was no apparent pre-inspiratory activity or oscillatory activity in 288 recorded GFAP<sup>+</sup> cells. However, we cannot entirely rule out low amplitude calcium oscillations. Previous recordings from astrocytes in preBötC brainstem slices employed the high-affinity indicator Oregon Green BAPTA 1 ( $K_d = 170\text{nM}$ ) whereas we used the medium-affinity indicator Asante Calcium Red ( $K_d = 400\text{nM}$ ). Previously reported astrocytic fluctuations that were of small amplitude ( $<1\% \Delta F/F_0$ ) and only visible after filtering (Oku et al., 2015). It is therefore plausible that we failed to detect astrocytic fluctuations due to experimental limitations related to our green GFAP reporter strain coupled with a red calcium dye of limited sensitivity. Further, the tight proximity of cell layers in culture conveniently allows many cells to be recorded simultaneously with less light scattering due to tissue thickness, but the signal is likewise prone to contamination by neuronal activity that is marginally out of focus yet still of a greater magnitude than any glial signals, which may be especially true at higher magnification. Finally, it is possible that astrocytes in this case were inadequately labeled due to loading feasibility of the indicator dye, or that they simply behave differently in a culture environment.

Whole-cell electrophysiology data show neurons in the ventral oscillatory group of brainstem-cerebellar co-cultures whose behavior appears similar to previously described rhythmic neurons in the preBötC of acute slices (Funk and Greer, 2013; Ramirez et al., 2012). These neurons receive periodic inspiratory drive potentials that generally produce bursts of action potentials with an underlying burst envelope that is larger at rest than at hyperpolarized potentials (Fig. 1.6B), suggesting that voltage-, or calcium-dependent conductances amplify the synaptic drive (Ramirez et al., 2012). The drive potentials had a duration of ~350 ms, which compares to the ~870 ms half-amplitude duration of the calcium signal in individual neurons, illustrating that the shape and time course of the calcium signal also depend on cellular calcium kinetics. Taken in conjunction with calcium imaging data and retrograde tracing with biocytin, we conclude that organotypic cultures retain a rhythmically active ventral network that corresponds to the preBötC. Its activity pattern spans dorsally into regions such as the intermediate reticular formation, the nucleus tractus solitarius, and the XII nucleus, which are associated with premotor and motor circuits that serve respiration. Midline activity also appears to correspond with the raphe obscurus (Ptak et al., 2009). Decreased tissue thickness and consequently the ability to capture many active neurons in the same focal plane with significantly reduced fluorescence scattering likely accounts for the increase in signal amplitude in cultures (both brainstem slice cultures and brainstem-cerebellar co-cultures) compared to acute slices. However, the existence of rhythmic neurons in the ventrolateral slice culture, and adjacent dorsomedial regions, does not necessarily guarantee that these neurons

correspond one-to-one to preBötC interneurons and respiratory premotor or motor neurons, or that they have not modified their behavior or physiology in some way. A degree of synaptic remodeling certainly occurs over time in vitro—we can see promiscuous fibers projecting between cerebellar and brainstem explants via retrograde biocytin tracing. Thus, we cannot exclude that circuits not found in the intact animal or unnatural strengthening of existing circuits develop over time in the cultures, which certainly should be taken into consideration when using this preparation. However, general synaptic connectivity between contralateral and dorsomedial motor regions of the slice appears to be preserved and, more importantly, the calcium activity in preBötC cultures reflects a consistent rhythmic pattern—initiation in the ventral oscillatory group followed by fast bilateral synchronization and subsequent propagation of signal to dorsomedial regions. Pharmacological modulation of the rhythm using agonists for NK1 and  $\mu$ -opioid receptors also mimics responses seen in acute slice (Gray et al., 1999), demonstrating that essential peptidergic modulating systems are intact in the cultures, at least at the postsynaptic level.

Thus, the preBötC slice culture preparation could be a useful model of respiratory rhythm generation that approximates the already widely used acute slice preparation and is amenable for optical and electrical stimulation and recording. The longevity of the culture preparation will facilitate molecular biological experiments and techniques, as well as any protocol that requires pharmacological perturbations lasting multiple days or weeks.

## **1.4 METHODS**

### **Ethical approval**

The Department of Experimental Medicine at the Panum Institute approved all experiments and procedures according to protocols laid out by Danish Ministry of Justice and the Danish National Committee for Ethics in Animal Research.

### **Organotypic slice cultures**

US Naval Medical Research Institute (NMRI) mice post-natal ages 0.5 to 5.5 days were anesthetized with isoflurane and immediately dissected in sterile-filtered chilled artificial cerebrospinal fluid (ACSF) containing (in mM): 184 glycerol, 2.5 KCl, 1.2 NaH<sub>2</sub>PO<sub>4</sub>, 30 NaHCO<sub>3</sub>, 20 HEPES, 25 D-glucose, 5 sodium ascorbate, 2 thiourea, 3 sodium pyruvate, 10 MgSO<sub>4</sub>, 0.5 CaCl<sub>2</sub>; pH 7.3, equilibrated by bubbling with carbogen (95% O<sub>2</sub> and 5% CO<sub>2</sub>). We cut transverse slices of the brainstem, 400 µm in thickness, at the level of the preBötC on a vibratome (Thermo Scientific Microm 650V, Waltham MA, USA) as described by newborn mouse atlases of the brainstem (Ruangkittisakul et al., 2011, 2014). Additionally, we often retained 400-µm-thick parasagittal slices of the cerebellum from the same mouse brain for co-culturing. For Stoppini-type cultures, transverse brainstem slices were placed onto semi-porous culture well inserts (Millipore PIC03050, Darmstadt, Germany) with cerebellar explants co-cultured along their dorsolateral borders. Mounted preparations were maintained in sterile-filtered organotypic culture media containing: 50% Eagle's MEM with Earle's Salts, 25% Hank's balanced salt solution, 25% heat-inactivated horse serum, 2 mM glutamine, 200 U/ml penicillin, 5 µg/ml streptomycin, 10 mM HEPES and an additional 3.6 mM D-glucose. The

cultures were treated with 10  $\mu$ M MK-801, an NMDA receptor antagonist, for the first three days in vitro. Fresh culture media was supplied every 48 hours thereafter until experimentation. These slices were then kept in a sterile humidified incubator at 35° C and atmospheric CO<sub>2</sub> concentrations during incubation.

We prepared some cultures according to the roller-drum technique, wherein the slices were placed on a coverslip embedded in citrated chicken plasma (Sigma-Aldrich, St. Louis, MO, USA) that was then coagulated by adding a drop of 100-150 U/ $\mu$ L thrombin (Sigma-Aldrich). The cultures were kept in sealed plastic tubes (flat bottom, NUNC Thermo Scientific, Waltham MA, USA) and placed in a rotating roller-drum (15 revolutions/h) at 35° C in humidified air. All procedures were performed in a sterile work environment within a Class 1 biosafety cabinet. The success rate in obtaining oscillating cultures depended in particular on the dissection experience and skill of experimenter, and approached 100% after ~3 months of training.

The thickness of the cultures was measured in counterstained sections using a Zeiss Axiolab microscope: The culture was drop fixed overnight in 4% paraformaldehyde, washed in Sørensen's Phosphate Buffer (0.1 M), dehydrated with increasing ethanol, embedded in Epon (EMBed-812, Electron Microscopy Sciences, PA, USA), cut in 3  $\mu$ m sections at a 90 degrees angle relative to the surface on a microtome, counter stained with 0.1% Toluidine (Sigma-Aldrich), and mounted with the mounting medium, Eukitt (Sigma-Aldrich).

### **GFAP+ mice**

Mice expressing enhanced green fluorescent protein (EGFP) under the promoter of glial fibrillary acidic protein [GFAP; line Tgn(hgFAPEGEP) GFEC 335] were kindly provided by Professor Frank Kirchhoff at the University of Saarland in Homburg, Germany (Lalo et al., 2006).

### **Electroporation**

Glass micropipettes were pulled from filamented capillary glass (outer diameter 1.5 mm, inner diameter 0.86 mm, Harvard Apparatus, Holliston, MA, USA) using a PUL-100 micropipette puller (World Precision Instruments, Sarasota, FL, USA), giving a tip diameter of 1-3  $\mu\text{m}$ . Pipettes were filled with 1% biocytin, 1 M KCl, 0.126 M Tris, placed in the slice culture, and positive current was applied in 50 ms pulses of 200  $\mu\text{A}$  at 2 Hz for 10 min. Current pulses were generated by a stimulus isolation unit gated by a waveform generator (IsoFlex and Master-8, A.M.P.I., Jerusalem, Israel).

### **Calcium imaging, and peptidergic compounds**

Loading solutions for membrane-permeable calcium indicators were prepared by combining 30  $\mu\text{l}$  of a 10 mM stock solution containing either Fluo-8 AM in DMSO (AAT Bioquest, Sunnyvale, CA) or Asante Calcium Red AM in DMSO (TEFLabs, Austin, TX, USA) with 3.5  $\mu\text{l}$  cremophore EL (Fluka, St. Louis, MO, USA) and 7.5  $\mu\text{L}$  of 20% pluronic acid in DMSO (AAT Bioquest, Sunnyvale, CA, USA). This 41  $\mu\text{l}$  of dye solution was then dissolved in 1.5 ml of a standard artificial cerebrospinal fluid solution (ACSF) containing 10  $\mu\text{M}$  MK-571 (an ATP-binding cassette transporter blocker that improves calcium indicator dye uptake (Manzini et al.,

2008). The ACSF consisted of (in mM): 129 NaCl, 3 KCl, 25 NaHCO<sub>3</sub>, 5 KH<sub>2</sub>PO<sub>4</sub>, 30 D-glucose, 0.7 CaCl<sub>2</sub>, 0.4 MgSO<sub>4</sub>, 100 mM D-mannitol, which was aerated by bubbling with carbogen (95% O<sub>2</sub> and 5% CO<sub>2</sub>) at room temperature. The final Fluo-8 AM (or Asante Calcium Red) concentration was 20 μM. Slice cultures were submerged in bubbled loading solution for 30-60 minutes before recording.

Fluorescent calcium activity was recorded in the slice culture using a stereo microscope (Leica MZ16 FA, Wetzlar, Germany) 30 min after the preparation was placed in a 2-ml recording chamber at 29° C, and perfused at 2 ml/min with preheated oxygenated ACSF. Light-emitting diodes (LEDs, HLV series, CCS LED Spotlight, Kyoto, Japan) and a metal-halide light source (Leica EL6000) illuminated the preparation. Appropriate filter sets for green fluorescence (Leica GFP3: excitation band-pass 450-490 nm and emission band-pass 500-575 nm) were inserted in the light path for fluorescence imaging. Time series acquisition was performed with an electron-multiplying charge-coupled device (EMCCD) camera (LucaEM S DL-658M, Andor Technology, Belfast, United Kingdom) at 10-129 Hz, controlled by SOLIS software (Andor Technology).

For cellular-level fluorescence detection, a metal halide light source PhotoFluor II (89North, Burlington, USA) or a LED light source, M470L2 (Thorlabs, Newton, NJ, USA) was coupled to a fixed-stage upright microscope via a liquid light guide and appropriate optical filters (for Fluo-8 AM, a modified Olympus U-MWIB set: excitation 457-487 nm, dichroic mirror 505 nm, emission 515-550 nm. For Asante Calcium Red AM, an Olympus U-MWIG2 set: excitation 520-550 nm, dichroic mirror 565 nm, emission BA580IF nm). Images were captured by an sCMOS

camera (Neo DC-152Q, Andor Technology) controlled by the SOLIS software (Andor Technology). Imaging protocols employed a 10x (NA 0.3), 20x (NA 0.5), 40x (NA 0.8), and 63x (NA 0.95) water immersion objectives. Time series images were acquired at 10-50 frames/s.

The NK1-receptor agonist Substance P acetate salt hydrate (SP), and  $\mu$ -opioid agonist [D-Ala<sup>2</sup>, N-Me-Phe<sup>4</sup>, Gly<sup>5</sup>-ol]-Enkephalin acetate salt (DAMGO, Sigma-Aldrich) were dissolved in water and further diluted in ASCF to give final concentrations of 500 nM and 1  $\mu$ M respectively. The effect of Substance P and DAMGO on burst frequency was tested in cumulative dosing measuring burst frequency over 20 s image stack in the control, 10 min of bath applied Substance P, and 10 min of Substance P plus DAMGO.

### **Whole-cell patch clamp**

Patch recordings employed an AxoClamp 2B amplifier (Molecular Devices, Sunnyvale, CA, USA) and ROE-200 micromanipulators (Sutter Instruments, Novato, CA, USA). Glass patch pipettes were pulled as described above to a tip resistance of 9-11 M $\Omega$ . Pipettes were loaded with a patch solution containing (in mM): 165 potassium D-gluconate, 10 NaCl, 0.5 MgCl<sub>2</sub>, 10 HEPES, 0.4 GTP, 4 ATP, 0.5 EGTA, pH 7.3, and then visually guided to target cells using a fixed-stage upright microscope (modified Olympus BX51) with a 63x (NA 0.95) objective. Data were digitally acquired at 20 kHz. Rhythmically active neurons were first recorded with the minimum necessary current bias to achieve stable activity with little spontaneous firing during inter-burst intervals.

## **Analysis and statistics**

Optical and electrophysiological data were analyzed offline using Igor Pro v. 6.36 (Wavemetrics, Lake Oswego, USA), Clampex 10.3 (Molecular Devices), and ImageJ v.1.49 (Schneider et al., 2012). Change in fluorescence over baseline fluorescence intensity ( $\Delta F/F_0$ ) was calculated using a moving Z-projection that finds minimum values of fluorescence across consecutive 1-s time windows throughout an image stack. The 1-s running average, uniquely calculated for each individual frame, was subtracted from it, throughout the time series to isolate fast calcium fluctuations from background fluorescence. Image stacks were then Kalman filtered to reduce noise and pseudo-colored ('rainbow' RGB look-up-table, red: maximum values of  $\Delta F$ , green: medium values of  $\Delta F$ , blue: minimum values of  $\Delta F$ ). Pixels were binned (mean of adjacent 2x2-10x10 points) and brightness and contrast were enhanced using ImageJ. In some experiments regions of interest (ROIs) were defined and average  $\Delta F$  values within a given ROI were plotted versus time. Unless otherwise stated, statistical values are given as mean  $\pm$  S.D. Student's t-test was used for statistical comparisons of two sample populations and ANOVA when more than two sample populations are compared. All statistical tests were performed using Origin 2015 (OriginLab Corp., Northampton, MA, USA).

## 1.5 REFERENCES

- Apuschkin, M., Ougaard, M., and Rekling, J.C. (2013). Spontaneous calcium waves in granule cells in cerebellar slice cultures. *Neurosci.Lett.* 553, 78–83.
- Bouvier, J., Thoby-Brisson, M., Renier, N., Dubreuil, V., Ericson, J., Champagnat, J., Pierani, A., Chédotal, A., and Fortin, G. (2010). Hindbrain interneurons and axon guidance signaling critical for breathing. *Nat. Neurosci.* 13, 1066–1074.
- Del Negro, C.A., Hayes, J.A., and Rekling, J.C. (2011). Dendritic Calcium Activity Precedes Inspiratory Bursts in preBötzinger Complex Neurons. *J. Neurosci.* 31, 1017–1022.
- De Zeeuw, C.I., Hoebeek, F.E., and Schonewille, M. (2008). Causes and consequences of oscillations in the cerebellar cortex. *Neuron* 58, 655–658.
- Feldman, J.L., Del Negro, C.A., and Gray, P.A. (2013). Understanding the rhythm of breathing: so near, yet so far. *Annu. Rev. Physiol.* 75, 423–452.
- Funk, G.D., and Greer, J.J. (2013). The rhythmic, transverse medullary slice preparation in respiratory neurobiology: Contributions and caveats. *Respir. Physiol. Neurobiol.* 186, 236–253.
- Gahwiler, B.H. (1981). Organotypic monolayer cultures of nervous tissue. *J.Neurosci.Methods* 4, 329–342.
- Gray, P.A., Rekling, J.C., Bocchiaro, C.M., and Feldman, J.L. (1999). Modulation of Respiratory Frequency by Peptidergic Input to Rhythmogenic Neurons in the PreBötzinger Complex. *Science* 286, 1566–1568.
- Gray, P.A., Hayes, J.A., Ling, G.Y., Llona, I., Tupal, S., Picardo, M.C.D., Ross, S.E., Hirata, T., Corbin, J.G., Eugénín, J., et al. (2010). Developmental origin of preBötzinger complex respiratory neurons. *J. Neurosci. Off. J. Soc. Neurosci.* 30, 14883–14895.
- Hartel, K., Schnell, C., and Hulsman, S. (2009). Astrocytic calcium signals induced by neuromodulators via functional metabotropic receptors in the ventral respiratory group of neonatal mice. *Glia* 57, 815–827.

- Hartelt, N., Skorova, E., Manzke, T., Suhr, M., Mironova, L., Kugler, S., and Mironov, S.L. (2008). Imaging of respiratory network topology in living brainstem slices. *MolCell Neurosci* 37, 425–431.
- Hulsmann, S., Oku, Y., Zhang, W., and Richter, D.W. (2000). Metabolic coupling between glia and neurons is necessary for maintaining respiratory activity in transverse medullary slices of neonatal mouse. *Eur.J.Neurosci.* 12, 856–862.
- Katona, G., Kaszas, A., Turi, G.F., Hajos, N., Tamas, G., Vizi, E.S., and Rozsa, B. (2011). Roller Coaster Scanning reveals spontaneous triggering of dendritic spikes in CA1 interneurons. *Proc.Natl.Acad.Sci.U.S.A* 108, 2148–2153.
- Koshiya, N., and Smith, J.C. (1999). Neuronal pacemaker for breathing visualized in vitro. *Nature* 400, 360–363.
- Koshiya, N., Oku, Y., Yokota, S., Oyamada, Y., Yasui, Y., and Okada, Y. (2014). Anatomical and functional pathways of rhythmogenic inspiratory premotor information flow originating in the pre-Botzinger complex in the rat medulla. *Neuroscience* 268, 194–211.
- Lalo, U., Pankratov, Y., Kirchhoff, F., North, R.A., and Verkhratsky, A. (2006). NMDA receptors mediate neuron-to-glia signaling in mouse cortical astrocytes. *J.Neurosci.* 26, 2673–2683.
- Manzini, I., Schweer, T.-S., and Schild, D. (2008). Improved fluorescent (calcium indicator) dye uptake in brain slices by blocking multidrug resistance transporters. *J. Neurosci. Methods* 167, 140–147.
- Oku, Y., Fresemann, J., Miwakeichi, F., and Hulsmann, S. (2015). Respiratory calcium fluctuations in low-frequency oscillating astrocytes in the pre-Botzinger complex. *RespirPhysiol Neurobiol.*
- Onimaru, H., and Homma, I. (2003). A novel functional neuron group for respiratory rhythm generation in the ventral medulla. *J.Neurosci.* 23, 1478–1486.
- Picardo, M.C.D., Weragalaarachchi, K.T.H., Akins, V.T., and Del Negro, C.A. (2013). Physiological and morphological properties of Dbx1-derived respiratory neurons in the pre-Böttinger complex of neonatal mice. *J. Physiol.* 591, 2687–2703.

- Ptak, K., Yamanishi, T., Aungst, J., Milesco, L.S., Zhang, R., Richerson, G.B., and Smith, J.C. (2009). Raphe neurons stimulate respiratory circuit activity by multiple mechanisms via endogenously released serotonin and substance P. *J.Neurosci.* 29, 3720–3737.
- Ramirez, J.M., Doi, A., Garcia, A.J., III, Elsen, F.P., Koch, H., and Wei, A.D. (2012). The cellular building blocks of breathing. *Compr.Physiol* 2, 2683–2731.
- Ruangkittisakul, A., Panaitescu, B., and Ballanyi, K. (2011). K<sup>+</sup> and Ca<sup>2+</sup> dependence of inspiratory-related rhythm in novel “calibrated” mouse brainstem slices. *Respir. Physiol. Neurobiol.* 175, 37–48.
- Ruangkittisakul, A., Kottick, A., Picardo, M.C.D., Ballanyi, K., and Del Negro, C.A. (2014). Identification of the pre-Bötzinger complex inspiratory center in calibrated “sandwich” slices from newborn mice with fluorescent Dbx1 interneurons. *Physiol. Rep.* 2.
- Schneider, C.A., Rasband, W.S., and Eliceiri, K.W. (2012). NIH Image to ImageJ: 25 years of image analysis. *Nat.Methods* 9, 671–675.
- Schnell, C., Freseman, J., and Hulsman, S. (2011). Determinants of functional coupling between astrocytes and respiratory neurons in the pre-Botzinger complex. *PLoS.One.* 6, e26309.
- Smith, J.C., Ellenberger, H.H., Ballanyi, K., Richter, D.W., and Feldman, J.L. (1991). Pre-Botzinger complex: a brainstem region that may generate respiratory rhythm in mammals. *Science* 254, 726–729.
- Sternberger, N.H., Quarles, R.H., Itoyama, Y., and Webster, H.D. (1979). Myelin-associated glycoprotein demonstrated immunocytochemically in myelin and myelin-forming cells of developing rat. *Proc.Natl.Acad.Sci.U.S.A* 76, 1510–1514.
- Stoppini, L., Buchs, P.-A., and Muller, D. (1991). A simple method for organotypic cultures of nervous tissue. *J. Neurosci. Methods* 37, 173–182.
- Wang, X., Hayes, J.A., Revill, A.L., Song, H., Kottick, A., Vann, N.C., LaMar, M.D., Picardo, M.C., Akins, V.T., Funk, G.D., et al. (2014). Laser ablation of Dbx1 neurons in the pre-Botzinger complex stops inspiratory rhythm and impairs output in neonatal mice. *Elife.* 3, e03427.

## **CHAPTER 2: Dendrites of rhythmically active neurons in the preBötzinger complex contain an $I_A$ -like potassium current**

### **2.1 INTRODUCTION**

Breathing is essential for homeostasis. Therefore, the physiological properties of neural circuits that generate and control respiratory rhythm are of longstanding interest. The preBötzinger complex (preBötC) of the ventral medulla contains a network of excitatory interneurons that generate the rhythm for inspiratory breathing movements (Feldman and Del Negro, 2006; Feldman et al., 2013; Smith et al., 1991). preBötC neurons can be dichotomously subdivided into two classes, which differ with respect to membrane potential trajectory during the respiratory cycle and electroresponsive properties (Picardo et al., 2013; Reklings et al., 1996). During rhythmic activity, *type-1* preBötC neurons integrate synaptic drive and exhibit preinspiratory depolarization ~400 ms prior to inspiratory bursts. *Type-2* neurons integrate synaptic as well, but it occurs later in the cycle, and *type-2* neurons exhibit preinspiratory depolarization ~200 ms prior to inspiratory bursts (Reklings et al., 1996). Early preinspiratory activity in *type-1* neurons suggests that they may initiate recurrent excitation that leads inexorably to the

synchronized onset of inspiratory burst and thus be rhythmogenic (Rekling et al., 1996; Smith et al., 1990).

The biophysical basis for the synchronized and coordinated onset of activity across the rhythmic neuronal population (i.e. orderly network recruitment) initiated by *type-1* neurons has yet to be fully explained, but may be related to the presence of a transient outward  $I_A$ -like current, a defining feature of *type-1* neurons (Rekling et al., 1996). Transient outward potassium currents (i.e., A-currents,  $I_A$ ) exhibit a range of voltage-dependent and kinetic properties (Birnbaum et al., 2004). In the preBötC,  $I_A$  activates at subthreshold membrane potentials and fully inactivates at membrane potentials above -40 mV (Hayes et al., 2008). Pharmacological inhibition of  $I_A$  in the preBötC results in spurious burst generation at both the cellular and network levels, which the authors attributed to disorderly recruitment of rhythmogenic preBötC neurons during recurrent excitation that precedes the inspiratory burst in each cycle of the rhythm (Hayes et al., 2008).

Measured via dendritic patch-clamp and  $Ca^{2+}$  imaging,  $I_A$  is expressed at a high density on the dendrites of hippocampal pyramidal cells and cerebellar Purkinje cells, where it acts locally to inhibit excitatory responses like  $Ca^{2+}$  spikes (Hoffman et al., 1997; Kampa and Stuart, 2006; Otsu et al., 2014). Dendritic  $I_A$  limits the effect of excitatory inputs that are sparse or transient (or both). Conversely, dendritic  $I_A$  promotes robust post-synaptic responses to temporally summated excitatory input, which is long-lasting enough to inactivate  $I_A$  and thus

exert a more profound influence on membrane potential trajectory (Magee et al., 1998).

The amplitude of the drive potential underlying inspiratory bursts in rhythmic preBötC neurons depends on a calcium-activated non-specific cation current ( $I_{CAN}$ ), which can be activated by  $Ca^{2+}$  influx via voltage-gated channels or via intracellular  $Ca^{2+}$  release linked to group I metabotropic glutamate receptors (mGluRs) (Pace et al., 2007). Simultaneous dendritic application of AMPA and group I mGluR agonists, but not AMPA alone, amplifies excitatory input recorded at the soma (Pace and Del Negro, 2008), suggesting that excitatory input is amplified by intrinsic conductances on dendrites.

Temporally sparse spontaneous synaptic activity during the interburst interval could cause spurious burst generation, if such activity could also evoke  $I_{CAN}$ . However, a mechanism that selectively inhibits sparse synaptic inputs could prevent dendritic amplification, thus avoiding spurious bursts during the interburst interval. Fast-activating voltage-dependent outward current on dendrites can shunt sparse excitatory input, and might explain the aforementioned disordered behavior seen during network-wide blockade of  $I_A$  in rhythmically active slices. Thus, we hypothesize that  $I_A$  is expressed on dendrites in *type-1* neurons, in addition to being somatically expressed (Hayes et al., 2008). Here we utilize an organotypic slice culture containing the preBötC to investigate the contribution of  $I_A$  in rhythmically active preBötC neurons to influence transient depolarization along dendrites and find that loss of dendritically localized  $I_A$  significantly increases the amplitude of voltage-sensitive dendritic  $Ca^{2+}$  transients. These

phenomena demonstrate a possible mechanism by which dendritic  $I_A$  might filter synaptic input to *type-1* neurons, blocking sparse input yet permitting temporally and spatially summing inputs during the preinspiratory phase, which can inactivate  $I_A$ , to exert a more profound effect.

## 2.2 RESULTS

### **Establishment of two rhythmic neuron classes in organotypic cultures of the preBötC**

Neurons in organotypic slice cultures containing the preBötC retain rhythmic respiratory related behavior analogous to that seen in acute slice preparations and brainstem *en bloc* recordings (Forsberg et al., 2016; Funk and Greer, 2013; Phillips et al., 2016). However, it is not yet known whether rhythmically active preBötC neurons in culture retain the dichotomous membrane properties classified as *type-1* and *type-2* first characterized in acute slice recordings (Rekling et al., 1996). *Type-1* and *type-2* neurons are segregated based on membrane voltage trajectory during rhythmic behavior (e.g., pre-inspiratory activity) and the presence of either a transient outward current,  $I_A$ , or a hyperpolarization-activated inward current,  $I_h$ . *Type-1* neurons prominently feature  $I_A$ , lack  $I_h$ , and display a ramp-like increase in membrane potential, known as pre-inspiratory activity, beginning ~400 ms prior to the inspiratory burst. Conversely, *type-2* neurons lack  $I_A$ , express  $I_h$ , and display more latent pre-inspiratory activity ~200 ms prior to the inspiratory burst (Rekling et al., 1996). Motor nerve rootlets typically deteriorate in slice cultures after 6 to 7 days in vitro

(DIV), so here *type-1* and *type-2* neurons were differentiated based on the presence of either  $I_A$  or  $I_h$ , but not preinspiratory latency.

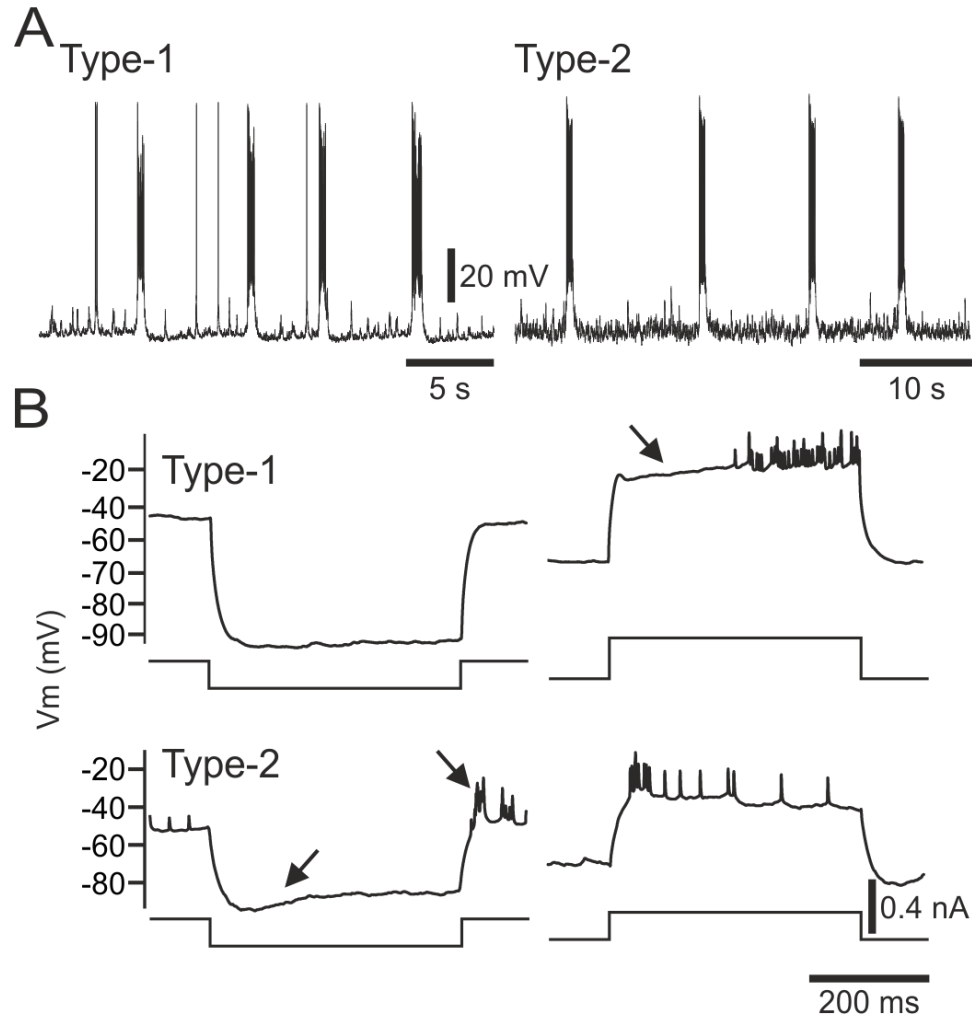


**Figure 2. 1** Electroresponsive properties of oscillating *type-1* and *type-2* neurons. **A:** Spontaneous oscillatory burst activity in two neurons recorded in current clamp mode. Note that the burst in the left-most neuron shows afterhyperpolarizations following the bursts. **B:** Hyperpolarizing and depolarizing square current pulses from around resting  $V_m$ , and from a slightly hyperpolarized membrane potential give rise to two distinctive electroresponsive responses in the two neurons. The *type-1* neuron show delayed excitation (arrow, top right trace), and the *type-2* neuron show sag-rebound potentials (arrows, lower left). Voltage traces are cycle-triggered averages of 5-10 sweeps, which truncates action potentials but retains the form of delayed excitation and ‘sag’ potentials.

Here we obtained whole-cell recordings from rhythmically active neurons in organotypic cultures containing the preBötC and tested the presence of both  $I_A$  and  $I_h$  in current clamp (Fig. 2.1,  $n = 42$ ). Rhythmic activity was first recorded using the minimum amount of negative holding current to inhibit spontaneous action potentials between rhythmic bursts (Fig. 2.1A, 0 to  $-0.15$  nA). Among all rhythmically active neurons, the mean burst interval was  $5.4 \pm 3.2$  s, and the mean burst duration was  $405 \pm 134$  ms ( $n = 42$ ).

The presence of  $I_A$  was determined by first hyperpolarizing neurons with negative holding current to a baseline membrane potential ( $V_m$ ) between  $-70$  mV and  $-80$  mV, which fully deinactivates  $I_A$  (Hayes et al., 2008). Square-wave positive current pulses of 400 ms duration were then delivered to evoke repetitive firing of action potentials. Neurons with  $I_A$  display a delay in membrane depolarization lasting 100-200 ms before firing repetitively, whereas neurons without  $I_A$  discharge action potentials throughout the duration of the current pulse without any notable delay exceeding the membrane time constant (Fig. 2.1B shows cycle-triggered averages of many sweeps to demonstrate the repeatability of delayed excitation or the lack thereof in *type-1* and *type-2* preBötC neurons).

The presence of  $I_h$  was determined by setting baseline  $V_m$  between  $-40$  and  $-50$  mV and delivering 400 ms negative current pulses of sufficient amplitude to hyperpolarize the neuron to  $-70$  to  $-90$  mV, which is sufficient to evoke  $I_h$  if it is expressed by the neuron. Neurons with  $I_h$  exhibit a 'sag' depolarization of  $\sim 10$  mV after being transiently hyperpolarized as well as a post-inhibitory rebound after the negative current pulse terminates (Fig. 2.1B shows cycle-triggered

averages of many sweeps to demonstrate the repeatability of 'sag' or the lack thereof in *type-1* and *type-2* preBötC neurons).

Among all recorded neurons we found 57% (n = 24) displayed *type-1* properties of delayed excitation (i.e.,  $I_A$ ) and lack of sag potential (i.e., no  $I_h$ ), while 31% (n = 13) displayed *type-2* properties of sag potentials ( $I_h$ ) and lack of delayed excitation (no  $I_A$ ). Of the remaining neurons, 7% (n = 3) showed both sag potential and delayed excitation, while 5% (n = 2) displayed neither  $I_A$  nor  $I_h$ . These results are in line with the distribution of respiratory neuron classes in acute slices (Picardo et al., 2013; Rekling et al., 1996). If we consider the null hypothesis to be that there is no relationship governing the expression of  $I_A$  and  $I_h$  in respiratory neurons, then the allotment of recorded neurons into *type-1* and *type-2* phenotypes is unlikely to have occurred by random chance (Fisher's exact test,  $p < 0.0001$ ), suggesting that the dichotomous electrophysiological properties of rhythmically active *type-1* and *type-2* neurons observed in the preBötC from acute slices, also persists in culture.

### **Voltage ramps during blockade of $I_A$ increase electrotonic compactness of *type-1* neurons**

To determine whether  $I_A$  might actively inhibit the spread of voltage transients along dendrites in *type-1* neurons, we next performed simultaneous single-electrode voltage clamp (SEVC) and fluorescent  $Ca^{2+}$ -imaging of rhythmically active neurons dialyzed with the fluorescent  $Ca^{2+}$  indicator, Fluo-8L (Fig. 2.2). This allowed us to track the relative amplitude of voltage changes at distal

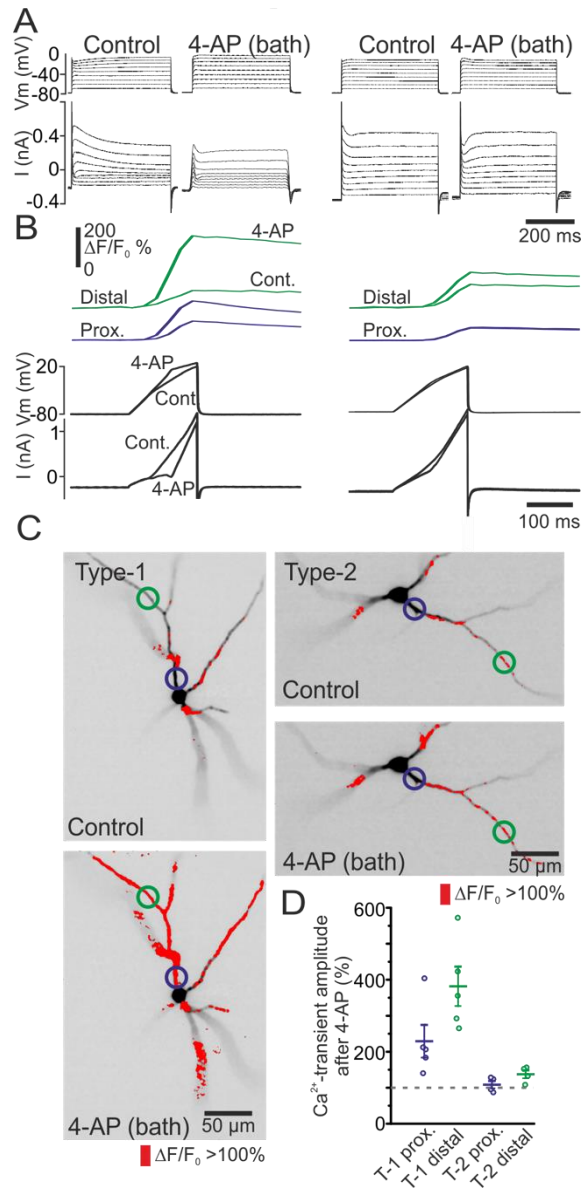


**Figure 2.** Bath applied 4-AP increases dendritic Ca<sup>2+</sup> transients in response to ramp depolarizations. **A:** Voltage clamp traces, with TTX (1 μM) in the perfusate, before and after adding 2 mM 4-AP to the bath. Left-most neuron shows a transient outward current, which is blocked by 4-AP thereby classifying the neuron as *type-1*. Right-most neuron shows no evidence of a transient outward current, classifying the neuron as a *type-2*. **B:** Ca<sup>2+</sup> transients in proximal and distal dendritic compartments in the two neurons in response to a 150 ms voltage ramp (-80 to 20 mV), and associated voltage and current traces. Responses before and after adding 2 mM 4-AP to the bath are overlaid. *Blue lines:* Proximal dendritic compartments. *Green lines:* Distal dendritic compartments. **C:** Live morphology of the two neurons with thresholded dendritic Ca<sup>2+</sup> transient amplitude overlaid in red. Red indicates Ca<sup>2+</sup> transient amplitudes (ΔF/F<sub>0</sub>) above 100%. **D:** Group data expressing the relative Ca<sup>2+</sup>-transient amplitude after 4-AP from all *type-1* (n=6) and *type-2* (n=5) neurons.

dendritic compartments using voltage-sensitive  $\text{Ca}^{2+}$  influx as a surrogate for direct measurements of membrane potential.

Since voltage clamping dendrites inherently suffers from a lack of space clamp as a function of distance from the recording pipette, changes in membrane potential enforced at the soma via SEVC would be attenuated at distal dendritic locations. The exact amount of that attenuation depends on passive cable properties (e.g. length, diameter, branch order) and density of voltage-gated conductances (Bar-Yehuda and Korngreen, 2008), but space-clamp error must be factored into data analysis and interpretation.

Neurons were first held at a command potential ( $V_C$ ) of -75 to -80 mV, well below the activation range of  $I_A$  but sufficiently negative to steady-state deinactivate the current (Hayes et al., 2008). The initial  $V_C$  was held constant for all stimulus protocols through the duration of each experiment. The presence of  $I_A$  was confirmed by delivering increasing 400 ms step commands up to +90mV (relative to  $V_C$ ). Neurons exhibiting a transient outward current that activated at subthreshold membrane potentials and inactivated above -40 mV after approximately 100-200 ms were considered to express  $I_A$  (Fig. 2. 2B).

Dendritic  $\text{Ca}^{2+}$  transients were then imaged during delivery of fast (150 ms duration) positive-going voltage ramps, starting at  $V_C$  and increasing to a final membrane potential capable of activating voltage-gated  $\text{Ca}^{2+}$  currents (mean =  $7.8 \pm 10.2$  mV,  $n = 9$ ). By using short-duration, quickly-increasing ramps we were able to elicit a supra-threshold  $\text{Ca}^{2+}$  response within the transient phase of

I<sub>A</sub> activation (Fig. 2. 2C). We then added 2 mM 4-AP to the bath perfusate and allowed 10 minutes for complete wash-in. Positive step commands as before were repeated to confirm blockade of I<sub>A</sub> (Fig. 2.2B) and dendritic Ca<sup>2+</sup> transients were imaged again while delivering the same voltage-ramps. The command stimulus was constant between control and 4-AP sweeps for each recorded neuron, but the peak amplitude achieved by the stimulus waveform (which is measurable in SEVC) nevertheless increased marginally across all neurons after addition of 4-AP because of increased effectiveness of the SEVC (*type-1*:  $8.5 \pm 2.2\%$ ,  $n = 5$ ; *type-2*:  $2.0 \pm 1.5\%$ ,  $n = 4$ ). Changes in peak amplitude of the stimulus waveform were significantly greater in *type-1* neurons than those in *type-2* neurons ( $n = 9$ ,  $p = 0.0017$ ). Input resistance in each cell was measured by taking the slope of the IV curve from the first 20 mV of increase above command potential—a range in which no apparent active conductances were elicited. Mean input resistance was  $221 \pm 97 \text{ M}\Omega$  in *type-1* neurons and was not significantly different in *type-2* neurons ( $181 \pm 77 \text{ M}\Omega$ ,  $n = 9$ ,  $p = 0.52$ ).

In order to visualize how voltage propagation through dendritic compartments is affected by a blockade of I<sub>A</sub>, we measured the relative increase in Ca<sup>2+</sup> indicator fluorescence ( $\Delta F/F_0$ ) evoked by voltage ramps before and after exposure to 4-AP (Fig. 2. 2D). Measurements were sampled from proximal dendritic compartments (less than or equal to 33  $\mu\text{m}$  from the soma) and distal dendritic compartments (greater than or equal to 69  $\mu\text{m}$  from the soma) with a minimum distance between measurement sites of 54  $\mu\text{m}$ . The mean proximal ROI distance from the soma was  $14 \pm 9 \mu\text{m}$  ( $n = 9$ ) and the mean distal ROI distance from the soma

was  $101 \pm 21 \mu\text{m}$  ( $n = 9$ ). The peak  $\Delta F/F_0$  values measured at each location were normalized to the amplitude of the control response in order to assess the relative change in fluorescence transient amplitude attributable to 4-AP effects (Fig. 2.2E). Among *type-1* neurons, the amplitude of fluorescent  $\text{Ca}^{2+}$  transients elicited by voltage ramps increased significantly at proximal regions by  $129 \pm 102\%$  ( $n=5$ ,  $p=0.023$ ) over the control amplitude and also increased significantly at distal regions by  $282 \pm 123\%$  ( $n=5$ ,  $p=0.003$ ). The increase at distal regions in *type-1* neurons was significantly greater than proximal regions ( $n = 10$ ,  $p=0.032$ ), suggesting a non-linear increase in the amplitude of calcium influx between perisomatic and distal dendritic compartments.

Among *type-2* neurons, the amplitude of fluorescent  $\text{Ca}^{2+}$  transients did not change significantly at proximal regions ( $10 \pm 22\%$ ,  $n = 4$ ,  $p = 0.22$ ) compared to control, while the amplitude at distal regions increased significantly by  $37 \pm 22\%$  ( $n = 4$ ,  $p = 0.022$ ). The increase in the ramp-evoked  $\text{Ca}^{2+}$  transient at distal regions in *type-2* neurons was not significantly greater than proximal regions ( $n = 8$ ,  $p = 0.064$ ) after 4-AP, which suggests that  $I_A$  does not play a significant role in governing dendritic depolarization of *type-2* preBötC neurons, particularly compared to their counterparts the *type-1* preBötC neurons (compare columns 1,2 to 3,4 in Fig. 2.2E).

These results demonstrate that a large increase in the voltage ramp-evoked  $\text{Ca}^{2+}$  transient occurs globally in *type-1* neurons when 4-AP-sensitive currents are blocked (Fig. 2.2D, depicting raw  $\Delta F/F_0$  values above 100%), and that this increase is greatest at distal dendritic regions. The data imply either: 1) blocking

$I_A$  diminishes the electronic decay of command voltages from the soma, which could be explained by removal of  $I_A$ -mediated shunting of the dendritic plasma membrane, or 2) blockade of  $I_A$  somehow increases recruitment of inward  $Ca^{2+}$  currents at distal dendritic sites. In either scenario articulated above, the data we present here cannot distinguish whether the observed changes in measured  $Ca^{2+}$  transient amplitude arise predominately from loss of somatic or dendritic  $I_A$ . Thus, we sought to determine whether ionic membrane currents could be blocked on distal dendritic sites while minimally affecting the soma.

### **Spatially-restricted application of channel blockers via iontophoresis**

To demonstrate that ion channels on selected sub-cellular regions of respiratory neurons in organotypic cultures can be pharmacologically manipulated, we conducted a positive control experiment in which  $Cd^{2+}$  was applied focally via iontophoresis to block  $Ca^{2+}$  channels in distal dendrites (Fig. 2.3). Simultaneous whole-cell patch-clamp and  $Ca^{2+}$ -imaging recordings were acquired from neurons in the preBötC of organotypic slice cultures. Spontaneous network activity was depressed to prevent spurious signals by reducing extracellular  $K^+$  concentration from 8 to 2.5 mM and increasing extracellular  $Ca^{2+}$  concentration from 1.5 to 2 mM in the recording ACSF. Membrane potential was held between -55 and -60 mV to prevent spontaneous spiking. A pipette containing an aqueous solution of 200 mM  $CdSO_4$  was positioned with a robotic manipulator under visual control so that its tip aimed at distal dendritic regions, while maintaining a -5 nA holding current to prevent ion leakage.

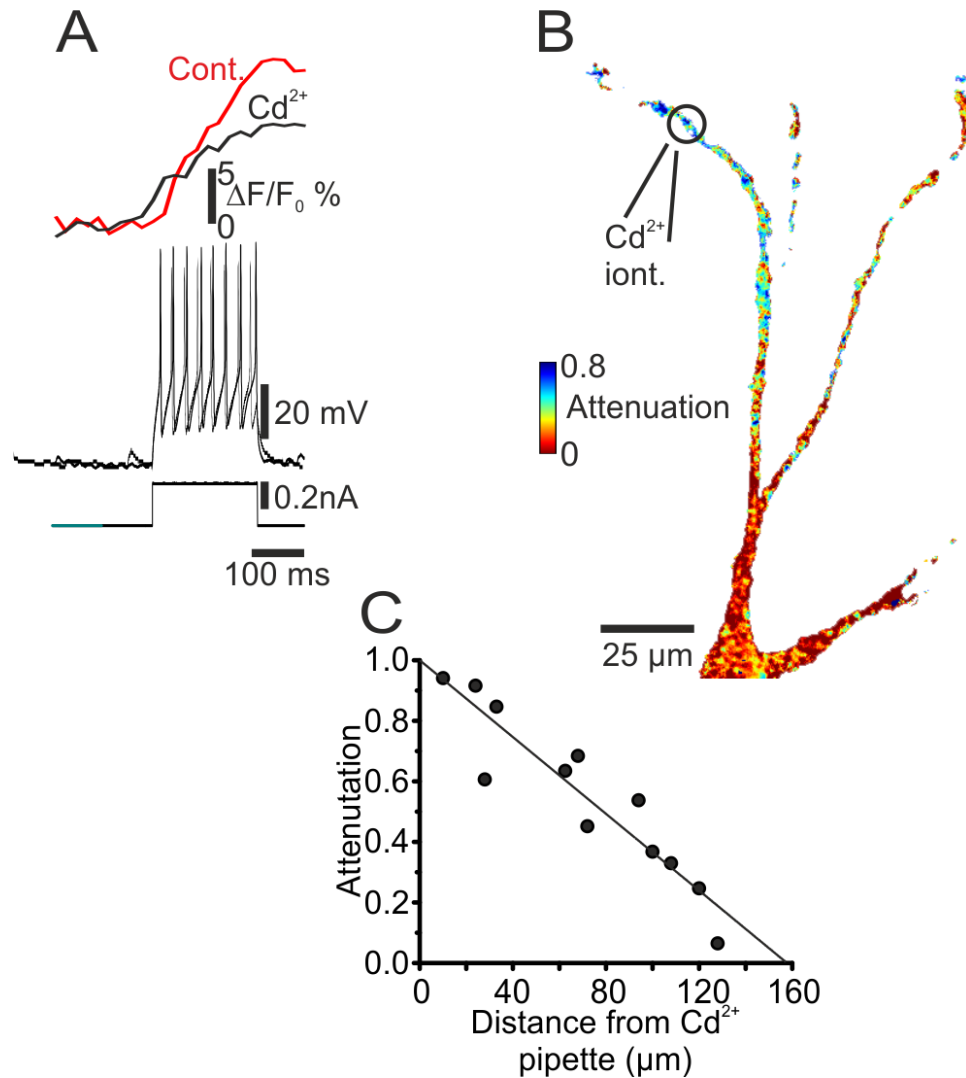


**Figure 2. 3** Dendritic iontophoresis of Cd<sup>2+</sup> reduce dendritic Ca<sup>2+</sup>-transients evoked by current pulses. A: 200 ms current pulses applied to a type-1 neuron evoking a spike train, and the resulting Ca<sup>2+</sup> transient in a dendritic compartment (red trace, ~130  $\mu$ m from soma, at the Cd<sup>2+</sup> application site). Iontophoresis of Cd<sup>2+</sup> (2 min, 500 ms pulses, 1 Hz) reduced the dendritic Ca<sup>2+</sup> transient (black trace). B: Same neuron as in A, showing the spatial distribution of the Cd<sup>2+</sup> effect, expressed as attenuation (Red: 0 to Blue: 0.8). Note that the site of application (pipette insert) has the largest attenuation compared to more proximal sites along the dendrite. C: Group data (n=7) showing the attenuation of spike-train evoked Ca<sup>2+</sup> transients in response to Cd<sup>2+</sup> as a function of distance along the dendrite towards the soma. Black line is a linear fit.

Positive current through the patch-recording pipette was then injected at the soma in either square-wave pulses (400 ms, 0.1-0.3 nA, 1 Hz), causing repetitive spiking, or short repetitive current pulses (3 ms, 0.8-1.2 nA, 100 Hz; Fig. 2.3A) evoking trains of 10 to 25 action potentials. The stimulus was maintained between control and drug application in each cell. After acquiring control sweeps, continuous ejection pulses were delivered to the iontophoretic pipette (400-500 ms, 1 Hz, +5-10 nA). After allowing 30-60 seconds for equilibration of drug ejection, we repeated the imaging sweeps. Peak  $\Delta F/F_0$  values were sampled from two locations in each cell, separated by a minimum of 50  $\mu\text{m}$  ( $n = 7$  neurons): proximal and distal dendritic regions as before, as well as the soma. The decrease in  $\text{Ca}^{2+}$  transient amplitude after application of  $\text{Cd}^{2+}$  was normalized to control sweeps.

Distance between the tip of the iontophoresis pipette and center of each ROI was measured in the xy-plane. Since both the iontophoresis pipette and imaged cellular compartments occupy approximately the same focal plane, the difference in their positions estimated the distance in three-dimensional space between the point of drug application and measurement. Regression analysis revealed a linear relationship between the degree of  $\text{Ca}^{2+}$  signal attenuation and straight-line distance from the pipette (Fig. 2.3C,  $n = 14$  measurements; y-intercept = 1.0,  $R^2 = 0.85$ ; ANOVA F-value = 64.45,  $p < 0.001$ ). This model suggests that less than 50% of the somatically evoked, dendritic  $\text{Ca}^{2+}$  transient is attenuated when the drug ( $\text{Cd}^{2+}$  in this case) is applied 79  $\mu\text{m}$  away from the ROI. Although the mobility in the extracellular environment due to applied electric field undoubtedly

differs between  $\text{Cd}^{2+}$  and 4-AP, both drugs are extracellular ion channel blockers that are not taken up by cellular processes. Thus, to ensure that recorded somata remained unaffected by iontophoretic drug application, we maintained a minimum of 96  $\mu\text{m}$  (and average of  $121 \pm 20 \mu\text{m}$ ,  $n = 12$  experiments) between the point of drug application and the nearest edge of somatic compartments in all subsequent local drug application experiments.

### **Dendritic $I_A$ blockade increases $\text{Ca}^{2+}$ response to somatically evoked stimuli in *type-1* neurons**

To determine whether increases in the  $\text{Ca}^{2+}$  response of *type-1* neurons due to 4-AP are mediated by dendritic  $I_A$ , we applied 4-AP via iontophoresis to distal dendrite sites (Fig. 2.4, mean dendritic length from soma:  $118 \pm 21 \mu\text{m}$ ,  $n = 12$ ) in rhythmically active preBötC neurons and measured the amplitude of  $\text{Ca}^{2+}$  transients in response to trains of 10 action potentials triggered by somatic current injection. Whole-cell patch-clamp recordings of rhythmically active neurons in the preBötC of slice cultures were acquired and their membrane properties were tested in current clamp recording mode to test for the presence of  $I_A$  and  $I_h$ , and thus determine whether they were *type-1* or *type-2*. At least 40 minutes after whole-cell break-in was allowed to pass for equilibration of dye diffusion at distal compartments. All imaging sweeps were performed in the presence of 2.5 mM  $\text{K}^+$  and 2 mM  $\text{Ca}^{2+}$ , which is the low-excitability ACSF as before.

We further added the ionotropic excitatory amino acid receptor antagonist NBQX (10-20  $\mu\text{M}$ ) to the perfusate to suppress excitatory network synaptic activity.

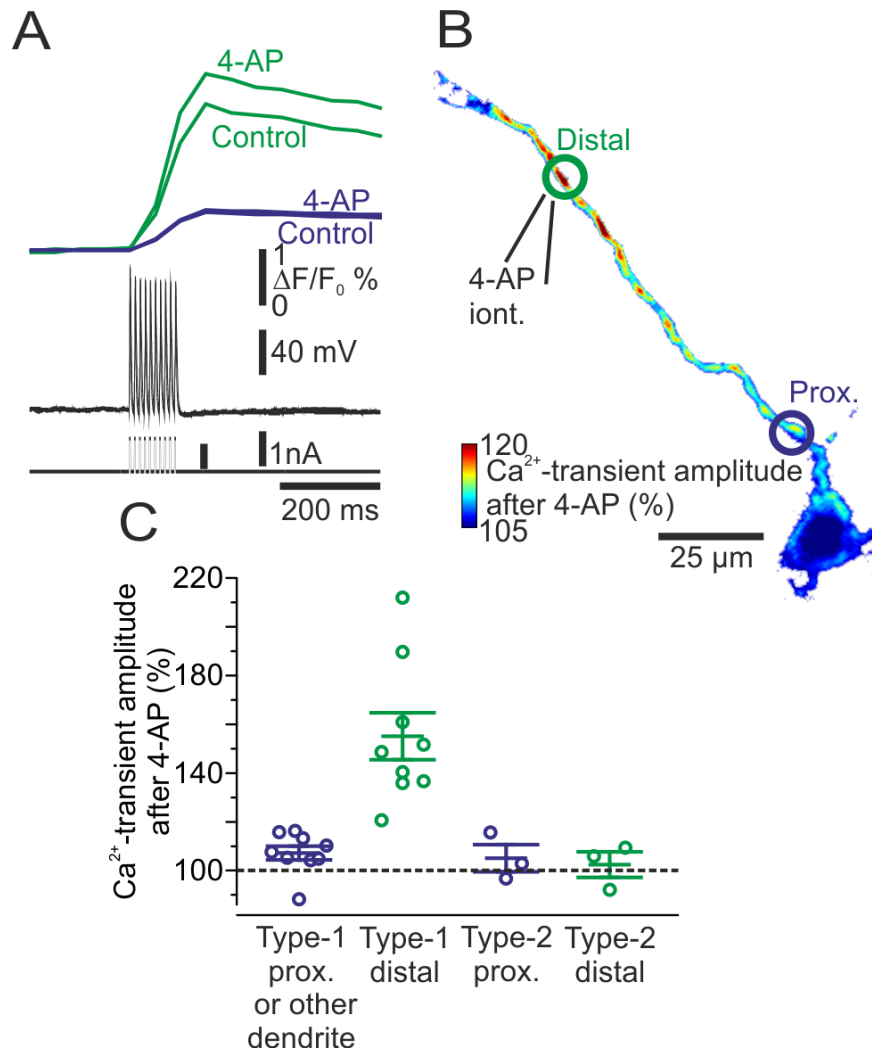


**Figure 2. 4** Dendritic iontophoresis of 4-AP increases dendritic Ca<sup>2+</sup> transients evoked by action potentials. **A:** A train of current pulses (10 pulses, 3 ms duration, 100 Hz) applied to a *type-1* neuron evoking 10 spikes. The resulting Ca<sup>2+</sup> transients in a dendritic compartment (~110  $\mu$ m from soma, placed next to the 4-AP pipette) are shown in **A**, displaying evoked responses before and after (overlaid green traces) iontophoresis of 4-AP (7 min, 500 ms pulses, 1 Hz). Transients in the same neuron sampled from a dendritic site close to soma (blue traces) before and after 4-AP applied distally. **B:** Same neuron as in **A**, showing the color coded spatial distribution of the 4-AP effect, expressed as Ca<sup>2+</sup> transient amplitude after 4-AP normalized to control (Blue: 105% to Red: 120%). Note that the site of application (pipette insert) has the largest increase in the Ca<sup>2+</sup> transient compared to more proximal sites along the dendrite. **C:** Group data showing the Ca<sup>2+</sup> transient amplitude after 4-AP application for dendritic sites that were either proximal or on other branches, and distal sites (i.e. in vicinity of the drug pipette) in both neuronal types (n=9 *type-1* neurons, and n=3 *type-2* neurons). Black dotted line is 100%, i.e. no change. Note that distal dendritic sites in *type-1* neurons show a large increase in Ca<sup>2+</sup>-transients after application of 4-AP.

In both control trials and local 4-AP application trials, ROIs were sampled from distal dendritic regions within 30  $\mu\text{m}$  of the iontophoresis pipette. To verify that the effects of 4-AP observed near the site of iontophoresis was caused by local ion channel blockade, we also sampled the relative change in fluorescence from a presumably unaffected compartment (i.e. other dendritic branches, proximal sites on the branch of drug application, and the soma) located at least 100  $\mu\text{m}$  away in the xy plane from the site of iontophoresis (mean distance:  $139 \pm 32 \mu\text{m}$ ,  $n = 12$ ). Pipettes containing 45 mM 4-AP dissolved in saline (165 mM NaCl, 0.2% Dextran-TMR, pH 7.5) were positioned at distal dendritic sites by visual guidance while maintaining a holding current of -5 nA to prevent drug leakage. During drug application trials, we applied continuous ejection pulses as before (400-500 ms, 1 Hz, +20-45 nA). In *type-1* neurons, spike train-evoked  $\text{Ca}^{2+}$  transients at distal dendritic sites (near the point of drug application) increased substantially by  $55 \pm 29\%$  (Fig. 2.4A-C,  $n = 9$ ,  $p = 2.16\text{E-}4$ ). Regions greater than 100  $\mu\text{m}$  from the site of iontophoresis also increased in  $\Delta F/F_0$  compared to the control response, which was also significant by statistical hypothesis testing but nonetheless represents a much less substantial change compared to the change measured in distal dendrites ( $7 \pm 8\%$ ,  $n = 9$ ,  $p = 0.017$ ). However, the increase at sites near the point of iontophoresis was significantly greater than on other dendritic branches or the soma (Welch's unequal variances t-test,  $n = 18$ ,  $p = 4.4\text{E-}4$ ).

*Type-2* neurons did not show a consistent increase at the site of iontophoresis (Fig. 2.4C,  $2 \pm 10\%$ ,  $n = 3$ ,  $p=0.34$ ) or at sites  $>100 \mu\text{m}$  from the site of iontophoresis ( $5 \pm 10\%$ ,  $n = 3$ ,  $p=0.23$ ). These results demonstrate that blockade

of  $I_A$  on dendrites has a substantial effect on the size of distal dendritic  $Ca^{2+}$  transients evoked by current pulses evoked at the soma in *type-1* preBötC neurons, but that  $I_A$  blockade has a negligible effect on dendritic  $Ca^{2+}$  transients evoked at the soma in *type-2* neurons.

## 2.3 DISCUSSION

A great deal is known about membrane properties of preBötC neurons, but almost all of that knowledge pertains to somatic ion channels and intrinsic membrane currents. We still lack a full understanding of how the active currents are distributed over the soma-dendritic membrane, including the dendrites where most of the synaptic input presumably arrives during respiratory network rhythmicity (Del Negro et al., 2011). Here we used organotypic slice cultures containing the preBötC to image  $Ca^{2+}$ -transients evoked by voltage increases propagating along extended dendritic lengths in rhythmically active neurons. The experiments show that an  $I_A$  is present in the dendrites of *type-1* neurons, which may influence synaptic integration.

The  $I_A$  found in *type-1* neurons of the preBötC likely influences the onset of the inspiratory burst phase during rhythmic network activity. Previous experiments show that bath applied 4-AP causes disordered inspiratory rhythms, and the  $I_A$  has been measured at the soma in whole-cell and outside-out patch-clamp recordings (Hayes et al., 2008). As such, excitatory input arriving at the soma is to some degree inhibited by  $I_A$  as long as the current is not steady-state inactivated. However, these previous measurements did not provide information

about the soma-dendritic distribution of  $I_A$ , which could influence how excitatory synaptic input is integrated both in the dendrites, and at the soma-axon hillock where spike initiation presumably occurs (Magee, 2000).

Interneurons in the preBötC lack the laminar organization, planar dendritic arborization, or large-diameter dendrites that have made other cell types (e.g. pyramidal cells) amenable to methods of investigating active properties in dendrites (e.g. dendritic patch-clamp or  $Ca^{2+}$  imaging). Organotypic slice cultures containing the preBötC flatten and become more translucent than acutely prepared slices after 6 to 7 days *in vitro*, which improve optical qualities of the tissue and reduces the degree to which neuronal processes traverse the z-axis (Gähwiler et al., 1997; Phillips et al., 2016). Cultures are thus better suited than acute slice preparations for dendritic  $Ca^{2+}$  imaging experiments. These slice cultures of the preBötC retain bilateral rhythmicity, respond to known network rhythm modulators, and contain neurons whose behavior resembles that found in acute preparations which have been well-established as models of respiratory rhythm generation for over 25 years (Feldman et al., 2013; Funk and Greer, 2013; Phillips et al., 2016; Ramirez et al., 2004; Reikling et al., 1996; Smith et al., 1991). However, it remains uncertain whether or not the respiratory-like rhythm found in slice cultures containing the preBötC arises from the same underlying cellular mechanisms as it does in acute slices that have been so widely exploited in studies of rhythm generation.

Membrane currents  $I_A$  and  $I_h$  can differentiate two distinct classes of rhythmically active neurons in the preBötC, dubbed *type-1* and *type-2* (Reikling et al., 1996).

We found that these currents are well-preserved in culture and maintain a similarly segregated distribution. That is, the majority of rhythmically active neurons feature exclusively  $I_A$  (i.e., *type-1*) or  $I_h$  (i.e., *type-2*), and few express both  $I_A$  and  $I_h$  or neither of these two. To better understand how *type-1* and *type-2* neurons integrate synaptic input, we asked whether  $I_A$  in rhythmically active neurons exists on dendrites and whether it has a significant impact on the ability for voltage to spread between somatic and distal dendritic compartments.

Blockade of  $I_A$  in *type-1* neurons results in a ~130% increase in the size of ramp-evoked  $Ca^{2+}$  transients at proximal dendritic regions and a ~280% increase at distal dendritic regions. In contrast, *type-2* neurons show no significant increase at proximal dendritic regions after bath application of 4-AP, while distal dendritic regions increased by ~40% over control. The global increase in the size of transients seen in *type-1* neurons reflects either a change in the electrotonic compactness of the neuron—more of the somatically-triggered depolarization propagates from the soma to the distal dendrite—or that somatically triggered depolarization is less counteracted by  $I_A$ . Both interpretations are feasible because  $I_A$  is an outward current whose polarity directly opposes depolarizing current longitudinally flowing from soma to dendrite and whose constituent ion channels in their open state may substantially change membrane impedance.

Bath application of 4-AP mediated a ~2-8% rise in the maximum amplitude of delivered voltage ramps in both *type-1* and *type-2* neurons, signifying a change in the strength of the SEVC. By some immeasurable degree, the consistent increase in ramp amplitudes definitely contributes to the observed change in

evoked transients on both proximal and distal dendrites. However, the error associated with *type-1* neurons (i.e. ~8%) was significantly greater than that seen in *type-2* neurons (i.e. ~2%), suggesting that blockage of  $I_A$  underlies a portion of the amplitude disparity. The strength of the SEVC, and by extension the ability to increase the membrane potential of the neuron, is thus correlated with the presence or absence of  $I_A$ , supporting the hypothesis that it affects either electrotonic compactness or resists membrane depolarization.

The observed increase in ramp-evoked  $Ca^{2+}$  transients in *type-1* neurons was also non-linear—distal sites increased ~2 fold more than proximal sites, suggesting that there is a disproportionate change in the amount of membrane depolarization occurring at distal versus proximal dendrites. Non-linear increases at distal dendritic locations could be explained as either an increase in the strength of space clamp mediated by the loss of  $I_A$  or the recruitment of active inward conductances at more distal dendritic sites (e.g. high-voltage activated  $Ca^{2+}$  channels). The possibility that active inward conductances may have been recruited at distal locations cannot be ruled out, particularly since *type-2* neurons also displayed non-linear response increases. However, space clamp issues are exacerbated by the presence of voltage-dependent membrane conductances on distal compartments (Bar-Yehuda and Korngreen, 2008). An inability to fully compensate for  $I_A$  during SEVC voltage ramps in *type-1* neurons indicates that these currents may be acting at a distance beyond the effective space clamp enforced near the soma. Ultimately, the explanation may be some combination of additional distally-located inward currents and an improved ability for SEVC to

clamp membrane potential further from the soma due to less inhibition of membrane depolarization caused by  $I_A$ , either somatically or also on dendrites.

The data from these experiments is unable to distinguish whether the apparent increase in electrotonic compactness, or reduced inhibition of membrane depolarization, is the result of solely somatic  $I_A$  or additionally includes dendritic  $I_A$ . To definitively determine whether the increases in the amplitude of ramp-evoked  $Ca^{2+}$  transients were caused by dendritic  $I_A$  in conjunction with somatic  $I_A$  we attempted to locally block  $I_A$  on dendrites of rhythmically active neurons such that the soma would not be affected.

The dendrites of rhythmically active interneurons in the preBötC have a span of less than 300  $\mu\text{m}$  (Picardo et al., 2013), and the maximum distance from the soma for which current injection evokes  $Ca^{2+}$  transients was 153  $\mu\text{m}$ . We employed iontophoretic drug ejection to ensure that we could restrict spread of ionic channel blockers applied at dendritic sites that were minimally 96  $\mu\text{m}$  away from the soma. We tested our ability to focally block channels by using  $Cd^{2+}$  as a positive control that would deliver complete knock-out of  $Ca^{2+}$  transients at the site of application. Since our recordings were capable of capturing  $>100$   $\mu\text{m}$  of dendritic structures within the same focal plane, we took measurements at two cellular locations in each time series from a total of  $n = 7$  neurons and pooled the data to generate a regression of signal attenuation against straight-line distance from the iontophoresis pipette (Fig. 2.3C). Although the ejection pipette was 96  $\mu\text{m}$  away from the soma in one experiment, the average distance between the iontophoresis pipette and soma was  $121 \pm 20$   $\mu\text{m}$ , which implies that the ejected

drug could only be 36% effective at the soma compared to the dendritic ROI, according to our linear model (Fig. 2.3C). The mobility which 4-AP and  $\text{Cd}^{2+}$  experience in an applied electric field differs, particularly since 4-AP does not carry a formal charge. While we were not able to precisely estimate the amount of 4-AP delivered to each cell, the control in  $\text{Cd}^{2+}$  rather serves to demonstrate how consistent drug delivery can be maintained at  $\sim 100 \mu\text{m}$  distances from the soma trial-by-trial. It is indeed likely that some amount of 4-AP reached the soma in our recordings, but the results nevertheless strongly suggest that  $I_A$  is present on dendrites where its effects are principally mediated.

Application of 4-AP to the dendrites of *type-1* neurons resulted in a  $\sim 55\%$  increase in spike train-evoked  $\text{Ca}^{2+}$  fluorescence at the site of iontophoresis and  $\sim 7\%$  increase in fluorescence in other compartments located either proximally on the same parent branch, at the soma, or on other dendritic branches occupying the same focal plane. The increase observed at other locations could indicate that the change in relative  $\text{Ca}^{2+}$  fluorescence observed at the site of iontophoresis is in part explained by some degree of 4-AP reaching the soma. However, the integrity of action potentials generated at the soma served as a final control. Bath application of 4-AP causes the half-width at maximum of action-potentials to increase by approximately 80% (Hayes et al., 2008). Here, we excluded trials wherein action potentials became distorted after drug application (a sign of either 4-AP reaching the soma or cell instability). Thus, these results indeed suggest that the density of ionic channels giving rise to  $I_A$

observed in *type-1* neurons of the preBötC extends well beyond the soma into distal dendritic compartments.

$I_A$  on the dendrites of rhythmically active preBötC neurons would be expected to counteract sparse excitatory synaptic events. It is important to distinguish that the enhancements in dendritic  $Ca^{2+}$  influx in the presence of 4-AP do not necessarily map one-to-one with a rise in voltage, but generally are indicative of changes in voltage, i.e., more  $Ca^{2+}$  influx indicates depolarization. The changes observed in ramp-evoked  $Ca^{2+}$  fluorescence were normalized to their control value in order to correct for confounds which could alter response linearity such as compartment volume, channel density, and the equilibrium of fluorescent indicator concentration (Yasuda et al., 2004). The non-linear increase in evoked  $Ca^{2+}$  transients at distal dendritic sites can be equally interpreted as a reduction in voltage decay between the soma and dendrites or as the recruitment of previously inhibited inward currents. Considering the overall global increase in  $Ca^{2+}$  response,  $I_A$  at minimum alters electrotonic compactness since all cellular compartments appear to charge in response to voltage stimuli more effectively. Propagation of voltage between sub-cellular compartments in *type-1* neurons appears to be significantly affected by the availability of  $I_A$  whereas *type-2* neurons have a more fixed relationship in the ability of transient somatic voltage increases to propagate through dendrites. Inactivation of  $I_A$ , which could be caused by sustained temporally-summed excitatory input, transitions *type-1* neurons from a relative low-excitability state, in which excitatory synaptic input is presumably inhibited by outward current (i.e.  $I_A$ ), to a high-excitability state that

appears to be significantly more electrotonically compact or resistant to membrane depolarization. This type of activity-dependent integration emphasizes why *type-1* neurons expressing  $I_A$  may be most critical in dictating the appropriately-timed onset of inspiratory burst cycles.

In conclusion, the subcellular distribution of  $I_A$  in *type-1* neurons extends to distal dendritic sites, and likely enforces a sublinear summation of input (i.e. EPSPs are inhibited) that is relieved by inactivation of  $I_A$ . This is evidenced by an apparent change in electrotonic compactness after blockade of  $I_A$  by 4-AP. During rhythmic network activity, steady-state inactivation of dendritic  $I_A$  could be achieved via building recurrent excitation during the pre-inspiratory phase of the inspiratory cycle. The presence of  $I_A$  in the dendrites of *type-1* neurons suggests that they are capable of limiting their excitability until network activity has grown during each respiratory cycle, and thus better suited for ordering the onset of inspiratory bursts.

## **2.4 METHODS**

### **Ethical approval**

The Department of Experimental Medicine at the Panum Institute approved all experiments and procedures according to protocols laid out by Danish Ministry of Justice and the Danish National Committee for Ethics in Animal Research.

### **Organotypic slice cultures**

US Naval Medical Research Institute (NMRI) mice post-natal ages P3.5 to P6.5 days were anesthetized with isoflurane and immediately dissected in sterile-

filtered chilled artificial cerebrospinal fluid (ACSF) containing (in mM): 184 glycerol, 2.5 KCl, 1.2 NaH<sub>2</sub>PO<sub>4</sub>, 30 NaHCO<sub>3</sub>, 5 HEPES acid, 15 HEPES base, 25 D-glucose, 5 sodium ascorbate, 2 thiourea, 3 sodium pyruvate, 10 MgSO<sub>4</sub>, 0.5 CaCl<sub>2</sub>; pH 7.3, equilibrated by bubbling with 95% O<sub>2</sub>/5% CO<sub>2</sub>. Transverse slices of the brainstem, 400 µm in thickness, were taken at the level of the preBötC using a vibrating microtome (Thermo Scientific Microm 650V, Waltham MA, USA). Anatomical markers, such as the principle loop of the inferior olive and obex of the fourth ventricle (Ruangkittisakul et al., 2011, 2014), were used to verify the rostral-caudal location of the preBötC and thus properly calibrate the slice. Cultures were prepared as previously described (Phillips et al., 2016) via the Stoppini interface method, placing transverse brainstem slices onto semi-porous culture well inserts (Millipore PIC03050, Darmstadt, Germany). Mounted preparations were maintained in sterile-filtered organotypic culture media containing: 50% Eagle's MEM with Earle's Salts, 25% Hank's balanced salt solution, 25% horse serum, 2 mM GlutaMAX (Gibco), 200 U/mL penicillin, 5 µg/mL streptomycin, 25 mM HEPES and an additional 3.6 mM D-glucose. The osmolarity of the culture medium measured 320-340 mOsm with a pH of 7.25. The cultures were treated with 10 µM MK-801, an NMDA receptor antagonist, for the first three days in vitro to prevent ischemia-related cell death (Newell et al., 1990). Fresh culture media was supplied every 48 hours thereafter until experimentation. These slices were then kept in a sterile, humidified incubator at 35° C and atmospheric CO<sub>2</sub> concentrations during incubation.

## **Electrophysiology**

Somatic whole-cell patch-clamp recordings were performed in current clamp and discontinuous single-electrode voltage clamp (dSEVC; sampling rate 1-2 kHz) using an AxoClamp 2B amplifier (Molecular Devices, Sunnyvale, CA, USA). Data were digitally acquired at a sampling rate of 10 kHz. Glass micropipettes were pulled from filamented capillary glass (O.D. 1.5 mm, I.D. 0.86 mm, Harvard Apparatus, Holliston, MA, USA) using a PUL-100 micropipette puller (World Precision Instruments, Sarasota, FL, USA) to a tip resistance of 4-6 M $\Omega$ . Patch pipettes were filled with a solution containing (in mM): 130 HCH<sub>3</sub>SO<sub>3</sub>, 130 KOH, 10 HEPES, 0.4 NaGTP, 4 Na<sub>2</sub>ATP, 5 Na<sub>2</sub>-phosphocreatine, 4 MgCl<sub>2</sub>, 0.05 Alexa 594 hydrazide (Invitrogen, Carlsbad, CA, USA), 0.1 Fluo-8L (AAT Bioquest, Sunnyvale, CA, USA). The osmolarity of the patch pipette solution measured 310 mOsm with a pH of 7.3. Patch pipettes were visually guided to target neurons under visual control using ROE-200 micromanipulators (Sutter Instruments, Novato, CA, USA) on a fixed-stage upright microscope (modified Olympus BX51, Olympus Corporation, Tokyo, Japan) under 40x magnification.

Iontophoresis was performed using a IP-X5 instrument (Neuro Data Instruments Corp., New York, NY, USA). Glass micropipettes were pulled as described above to a tip resistance of 8-10 M $\Omega$  for single-drug trials. For experiments involving 4-aminopyridine (4-AP) pipettes were filled with an aqueous solution containing: 165 mM NaCl, 10 mM HEPES, and 0.2% tetramethylrhodamine-dextran. For inhibition of I<sub>A</sub> localized to dendrites, we included 45 mM 4-AP (pH 7.5). For experiments involving local iontophoretic application of Cd<sup>2+</sup>, an aqueous solution

containing exclusively 200 mM CdSO<sub>4</sub> was used. ACSF in Cd<sup>2+</sup> experiments was free of phosphates to avoid precipitation. Pulses were delivered at 1 Hz (500 ms pulse duration) with the ejection currents: +20-30 nA to eject 4-AP, +5-10 nA to eject Cd<sup>2+</sup>.

During voltage-clamp recordings and dendritic glutamate iontophoresis, 1 μM TTX was added to the bath to block Na<sup>+</sup> current. A-current was blocked with bath-applied 2 mM 4-AP when not applied locally. During spike train response experiments, 10 μM 2,3-Dioxo-6-nitro-1,2,3,4-tetrahydrobenzo[f]quinoxaline-7-sulfonamide (NBQX) disodium salt (Tocris Bioscience, Bristol, UK) was added to the bath to block Ca<sup>2+</sup> transients arising from spontaneous excitatory synaptic transmission.

Rhythmic activity in slices was recorded in artificial cerebrospinal fluid (ACSF) containing (in mM): 124 NaCl, 3 KCl, 5 KH<sub>2</sub>PO<sub>4</sub>, 25 NaHCO<sub>3</sub>, 25 D-Glucose, 1 ascorbic acid, 1 MgCl<sub>2</sub>, 1.5 CaCl<sub>2</sub> with a pH of 7.4, equilibrated by bubbling with 95% O<sub>2</sub>/5% CO<sub>2</sub>. The final concentration of K<sup>+</sup> was [K<sup>+</sup>]<sub>o</sub> = 8 mM, which globally elevates resting membrane potentials and increases the frequency of spontaneous respiratory rhythm. To identify I<sub>A</sub> and I<sub>h</sub> in current clamp experiments, perfusion bath ACSF was exchanged after recording >15 minutes of rhythmic activity for a low excitability ACSF in which external K<sup>+</sup> concentration was reduced from 8 to 3 mM and external Ca<sup>2+</sup> was raised from 1.5 mM to 2 mM. These modifications reduced or stopped network rhythmic activity by globally hyperpolarizing neuronal membrane potentials and increasing the threshold for Na<sup>+</sup> channel activation (Panaitescu et al., 2009). Low excitability ACSF contained

(in mM): 124 NaCl, 2.5 KCl, 1.25 NaH<sub>2</sub>PO<sub>4</sub>, 25 NaHCO<sub>3</sub>, 25 D-glucose, 1 ascorbic acid, 1 MgCl<sub>2</sub>, 2 CaCl<sub>2</sub>, with a pH of 7.4, equilibrated by bubbling with 95% O<sub>2</sub>/5% CO<sub>2</sub>.

### **Ca<sup>2+</sup> imaging**

The region of the organotypic culture (see Fig. 2.1 in Phillips et al. 2016) containing the preBötC was targeted via anatomical landmarks and visualization of synchronized rhythmic network activity during whole-slice Ca<sup>2+</sup> imaging. The membrane-permeable fluorescent Ca<sup>2+</sup> indicator, Fura-2 AM (AAT Bioquest), was bath loaded prior to each experiment. Culture inserts were submerged in 1.5 mL of loading solution containing 35 µM of a 1 mM stock solution of Fura-2 AM in DMSO along with 0.05% pluronic acid dissolved in low excitability ACSF. Slices were incubated in loading solution at room temperature for 30-40 minutes then moved to the recording chamber and allowed 15 minutes of recovery and additional de-esterification prior to imaging and patching. Preheated and oxygenated ACSF was perfused into the recording chamber during recording at 2 ml/min and 29° C.

Fluorescent Ca<sup>2+</sup> activity was recorded in wide-field on a fixed-stage upright microscope (modified Olympus BX51), illuminated by a metal halide light source PhotoFluor II (89North, Burlington, USA) or a LED light source, M470L2 (Thorlabs, Newton, NJ, USA). Red and green channel fluorescence was visualized using a dual-bandpass filter set (Chroma 59022: excitation dual band-pass 450-490 nm/555-590 nm, emission dual band-pass 500-543 nm/603-665 nm). Red and green channels were separated during acquisition by manually

exchanging an additional excitation filter in the light train (Semrock FF01: band-pass 565-605 nm; Semrock FF02: band-pass 457-487 nm, Rochester, NY, USA). Time series acquisition was performed with a sCMOS camera (Neo DC-152Q, Andor Tehcnology, Belfast, UK) controlled by SOLIS software (Andor Tehcnology). Imaging protocols employed 10x (NA 0.3) and 40x (NA 0.8) water immersion objectives. Time series were acquired at 10-50 Hz. At least 30 minutes of perfusion was allowed after break-in during whole-cell patch clamp to allow equilibration of intracellular Ca<sup>2+</sup> dye. Dark current—the background sensor noise in the absence of illumination—was sampled prior to the start of each acquisition and subtracted from all imaging sweeps.

### **Data analysis**

Dendritic Ca<sup>2+</sup> transients were calculated as the percent change in fluorescence relative to baseline values ( $\Delta F/F_0$ ). Background was subtracted frame-by-frame, taken as the mean background fluorescence immediately adjacent to the dendritic ROI. Dendritic ROIs were hand drawn along neural processes, extending for no more than 10  $\mu\text{m}$  in length. The mean pre-stimulus fluorescence in the dendritic ROI was taken as  $F_0$ . For each condition, 4-6 sweeps were acquired with 10-30 second intervals, and subsequently averaged after calculation of  $\Delta F/F_0$ .

Electrophysiological data were acquired using pClamp 10.0 (Molecular Devices, Sunnyvale, CA, USA) and subsequently analyzed using custom scripts written in Igor Pro 6 (Wavemetrics, Tigard, OR, USA).

Unless otherwise stated, statistical values are given as mean  $\pm$  SD. Student's t-test was used for statistical comparisons of one- and two-sample populations. In cases where equal variance between samples could not be assumed, Welch's correction was applied and is indicated. Fisher's exact test was used to assess the distribution of neuronal membrane currents. All statistical tests were performed using Origin 9.1 (OriginLab Corp., Northampton, MA, USA).

## 2.5 REFERENCES

- Bar-Yehuda, D., and Korngreen, A. (2008). Space-Clamp Problems When Voltage Clamping Neurons Expressing Voltage-Gated Conductances. *J. Neurophysiol.* *99*, 1127–1136.
- Birnbaum, S.G., Varga, A.W., Yuan, L.-L., Anderson, A.E., Sweatt, J.D., and Schrader, L.A. (2004). Structure and Function of Kv4-Family Transient Potassium Channels. *Physiol. Rev.* *84*, 803–833.
- Del Negro, C.A., Hayes, J.A., and Rekling, J.C. (2011). Dendritic Calcium Activity Precedes Inspiratory Bursts in preBötzinger Complex Neurons. *J. Neurosci.* *31*, 1017–1022.
- Feldman, J.L., and Del Negro, C.A. (2006). Looking for inspiration: new perspectives on respiratory rhythm. *Nat. Rev. Neurosci.* *7*, 232–242.
- Feldman, J.L., Del Negro, C.A., and Gray, P.A. (2013). Understanding the rhythm of breathing: so near, yet so far. *Annu. Rev. Physiol.* *75*, 423–452.
- Forsberg, D., Horn, Z., Tserga, E., Smedler, E., Silberberg, G., Shvarev, Y., Kaila, K., Uhlén, P., and Herlenius, E. (2016). CO<sub>2</sub>-evoked release of PGE<sub>2</sub> modulates sighs and inspiration as demonstrated in brainstem organotypic culture. *eLife* *5*, e14170.
- Funk, G.D., and Greer, J.J. (2013). The rhythmic, transverse medullary slice preparation in respiratory neurobiology: Contributions and caveats. *Respir. Physiol. Neurobiol.* *186*, 236–253.
- Gähwiler, B.H., Capogna, M., Debanne, D., McKinney, R.A., and Thompson, S.M. (1997). Organotypic slice cultures: a technique has come of age. *Trends Neurosci.* *20*, 471–477.
- Hayes, J.A., Mendenhall, J.L., Brush, B.R., and Del Negro, C.A. (2008). 4-Aminopyridine-sensitive outward currents in preBötzinger complex neurons influence respiratory rhythm generation in neonatal mice. *J. Physiol.* *586*, 1921–1936.
- Hoffman, D.A., Magee, J.C., Colbert, C.M., and Johnston, D. (1997). K<sup>+</sup> channel regulation of signal propagation in dendrites of hippocampal pyramidal neurons. *Nature* *387*, 869–875.

- Kampa, B.M., and Stuart, G.J. (2006). Calcium Spikes in Basal Dendrites of Layer 5 Pyramidal Neurons during Action Potential Bursts. *J. Neurosci.* *26*, 7424–7432.
- Magee, J.C. (2000). Dendritic integration of excitatory synaptic input. *Nat. Rev. Neurosci.* *1*, 181–190.
- Magee, J., Hoffman, D., Colbert, C., and Johnston, D. (1998). Electrical and Calcium Signaling in Dendrites of Hippocampal Pyramidal Neurons. *Annu. Rev. Physiol.* *60*, 327–346.
- Newell, D.W., Malouf, A.T., and Franck, J.E. (1990). Glutamate-mediated selective vulnerability to ischemia is present in organotypic cultures of hippocampus. *Neurosci. Lett.* *116*, 325–330.
- Otsu, Y., Marcaggi, P., Feltz, A., Isope, P., Kollo, M., Nusser, Z., Mathieu, B., Kano, M., Tsujita, M., Sakimura, K., et al. (2014). Activity-dependent gating of calcium spikes by A-type K<sup>+</sup> channels controls climbing fiber signaling in Purkinje cell dendrites. *Neuron* *84*, 137–151.
- Pace, R.W., and Del Negro, C.A. (2008). AMPA and metabotropic glutamate receptors cooperatively generate inspiratory-like depolarization in mouse respiratory neurons in vitro. *Eur. J. Neurosci.* *28*, 2434–2442.
- Pace, R.W., Mackay, D.D., Feldman, J.L., and Del Negro, C.A. (2007). Inspiratory bursts in the preBötzinger complex depend on a calcium-activated non-specific cation current linked to glutamate receptors in neonatal mice. *J. Physiol.* *582*, 113–125.
- Panaitescu, B., Ruangkittisakul, A., and Ballanyi, K. (2009). Silencing by raised extracellular Ca<sup>2+</sup> of pre-Bötzinger complex neurons in newborn rat brainstem slices without change of membrane potential or input resistance. *Neurosci. Lett.* *456*, 25–29.
- Phillips, W.S., Herly, M., Negro, C.A.D., and Rekling, J.C. (2016). Organotypic slice cultures containing the preBötzinger complex generate respiratory-like rhythms. *J. Neurophysiol.* *115*, 1063–1070.
- Picardo, M.C.D., Weragalaarachchi, K.T.H., Akins, V.T., and Del Negro, C.A. (2013). Physiological and morphological properties of Dbx1-derived respiratory neurons in the pre-Bötzinger complex of neonatal mice. *J. Physiol.* *591*, 2687–2703.

- Ramirez, J.-M., Tryba, A.K., and Peña, F. (2004). Pacemaker neurons and neuronal networks: an integrative view. *Curr. Opin. Neurobiol.* 14, 665–674.
- Rekling, J.C., Champagnat, J., and Denavit-Saubie, M. (1996). Electroresponsive properties and membrane potential trajectories of three types of inspiratory neurons in the newborn mouse brain stem in vitro. *J. Neurophysiol.* 75, 795–810.
- Ruangkittisakul, A., Panaitescu, B., and Ballanyi, K. (2011). K<sup>+</sup> and Ca<sup>2+</sup> dependence of inspiratory-related rhythm in novel “calibrated” mouse brainstem slices. *Respir. Physiol. Neurobiol.* 175, 37–48.
- Ruangkittisakul, A., Kottick, A., Picardo, M.C.D., Ballanyi, K., and Del Negro, C.A. (2014). Identification of the pre-Bötzinger complex inspiratory center in calibrated “sandwich” slices from newborn mice with fluorescent Dbx1 interneurons. *Physiol. Rep.* 2.
- Smith, J.C., Greer, J.J., Liu, G.S., and Feldman, J.L. (1990). Neural mechanisms generating respiratory pattern in mammalian brain stem-spinal cord in vitro. I. Spatiotemporal patterns of motor and medullary neuron activity. *J. Neurophysiol.* 64, 1149–1169.
- Smith, J.C., Ellenberger, H.H., Ballanyi, K., Richter, D.W., and Feldman, J.L. (1991). Pre-Bötzinger Complex: A Brainstem Region That May Generate Respiratory Rhythm in Mammals. *Science* 254, 726–729.
- Yasuda, R., Nimchinsky, E.A., Scheuss, V., Pologruto, T.A., Oertner, T.G., Sabatini, B.L., and Svoboda, K. (2004). Imaging Calcium Concentration Dynamics in Small Neuronal Compartments. *Sci. Signal.* 2004, pl5–pl5.

## CONCLUSIONS

Breathing is vital to life, obviously, and understanding its neural origins is an important problem for physiology and neuroscience. Respiration is controlled by neuronal populations distributed throughout the brainstem, of which the preBötC is predominant as the source of the inspiratory rhythm, coordinating all other respiratory phases (e.g., post-inspiration and expiration) as well as most orofacial behaviors, e.g., whisking, sniffing, licking, chewing, and swallowing (Kleinfeld et al., 2014; Moore et al., 2013, 2014). To understand how breathing rhythm is generated, the brainstem has been reduced to isolate the most essential network circuitry necessary for rhythmogenesis (Funk and Greer, 2013; Reklings and Feldman, 1998; Smith et al., 1991; Suzue, 1984). This reductionist approach culminated in the development of acute medullary slice preparations, which isolate just the preBötC and sufficient premotor and motor neurons to generate rhythm and measurable inspiratory related motor output (Smith et al., 1991). These slices for over 25 years have substantially improved the ability of investigators to investigate the cellular and synaptic properties of respiratory interneurons, and have also been used profitably in molecular genetic analyses of these central circuits (Bouvier et al., 2010; Del Negro et al., 2002; Feldman et al., 2013; Gray et al., 1999, 2010; Reklings et al., 1996; Tan et al., 2008). However, acute medullary slices come with several caveats which have

restricted experimental design—namely, slices are at most viable for less than one day (Funk and Greer, 2013), and morphological characteristics of preBötC interneurons complicate studying synaptic integration in dendrites. The methodologies developed herein and experiments presented in this dissertation have attempted to ameliorate the drawbacks inherent in acute slice studies in order to both expand possible experimental approaches and to evaluate the role of a particular membrane conductance ( $I_A$ ) as it relates to a fundamental—but incompletely understood—component of inspiratory rhythm generation: integration of excitatory synaptic activity into inspiratory bursts occurs primarily in dendrites (Pace and Del Negro, 2008; Pace et al., 2007; Reikling et al., 1996).

Chapter 1 presented a novel organotypic slice culture containing the preBötC and demonstrates that its behavior closely resembles analogous acute slices. The rhythm is generated by surviving interneurons whose electrophysiological behavior, synaptic projections and frequency-modulating receptor types (i.e. neurokinin-1 receptors,  $\mu$ -opioid receptors) remain intact. Calcium imaging from these cultured preparations highlights improved optical qualities, allowing isolation of somatic calcium transients from up to 200 neurons at a time under 10x magnification and subcellular measurements of fluorescence intensity under 63x magnification (see Figure 1.3).

Organotypic slice cultures containing the preBötzinger complex are a useful alternative to acute slice preparations with the added advantage of 1 to 4 weeks of viability and improved optical qualities for imaging. By increasing the window of time in which experiments may be conducted, investigators can utilize

molecular techniques that require multi-day incubation periods (e.g. viral transduction of recombinant DNA or non-viral transfection of plasmid DNA). The ability to express genes of interest or exogenous DNA (e.g. coding for fluorescent proteins) and subsequently record from rhythmically active preparations is particularly useful to respiratory neurobiologists, permitting rapid identification of cell types of interest and the use of genetically encoded molecular tools (e.g. optogenetics). It is indeed possible to stereotaxically inject viral vectors carrying recombinant DNA (e.g., adenovirus) into the preBötC of living animals. However, such injections are typically performed in juvenile or adult mice and then assayed approximately one week later *in vivo* or histologically. Although cellular recordings of rhythmic activity have previously been achievable in acute slice preparations taken from juvenile mice, thicker tissue sectioning (e.g. ~700  $\mu\text{m}$ ) is required to capture the preBötC and hypoglossal motor nuclei in a single slice and such preparations do not reliably produce motor output beyond P21, making them more difficult to study (Funk et al., 1994; Ramirez et al., 1996). To the best of my knowledge, an adult slice that retains the preBötC and remains viable and rhythmically active *in vitro*, has not been accomplished. As such, the usefulness of acute slice preparations lies between embryonic stages up to P14 (realistically this window is limited to P4, and P14 is not nearly as advantageous for recording and imaging), which is well before targeted *in vivo* injections can affect respiratory circuits via transduction of recombinant DNA. Alternatively, transgenic animals can be used to express exogenous DNA or to modify genes of interest or express certain reporter proteins, but transgenic models require development of

at least one (and often two) viable mutant mouse strains for each experimental objective. Further, promoter-driven expression or knock-out occurs genome-wide, which modifies the entire brain and CNS experimental confounds. Thus, the options for vector DNA expression are limited for *in vitro* experiments. Organotypic slice cultures, on the other hand, do not suffer from these restrictions. Viral transduction has already been demonstrated in rhythmically active slice cultures containing the preBötC (Forsberg et al., 2016)(Fig. C.1; Rekling unpublished). Transfection in organotypic cultures also need not be viral-based nor ubiquitous. Plasmid DNA can be delivered non-virally (Murphy and Messer, 2001), in a region specific manner (Arsenault et al., 2014; Wickersham et al., 2007), or even to single cells via electroporation (Nguyen et al., 2012; Rathenberg et al., 2003). The usefulness of organotypic slice cultures containing the preBötC has likely only begun to be realized.

### **rAAV9.hSyn.TurboRFP.WPRE.rBG**

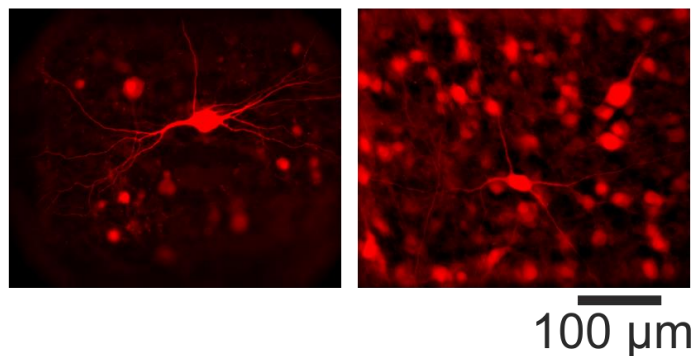


Figure C. 1 Adeno-associated viral transduction of red fluorescent protein in slice cultures containing the preBötC. Left panel: Cropped image focusing on strong expression of red fluorescent protein in a single neuron taken at 40x magnification. Note expression throughout the soma-dendritic morphology. Right panel: View of the same neuron uncropped. Note widespread expression of the red fluorescent protein in multiple cells.

Chapter 2 demonstrated that the subcellular distribution of a transient outward  $K^+$  current,  $I_A$ , extends onto the dendrites of *type-1* rhythmically active preBötC neurons. Dendritic  $I_A$  may inhibit excitatory input that occurs sparsely in rhythmic neurons, which would act to suppress these inputs (as long as  $I_A$  remains deinactivated). That scenario may characterize the interval between inspiratory bursts. Nonetheless, as activity increases among preBötC neurons, the temporal summation of repetitive input will cause steady-state inactivation of  $I_A$ , which would facilitate these inputs and promote synchronous burst generation in the network. Excitatory activity occurring when  $I_A$  steady-state inactivates experiences a lesser degree of current inhibition when propagating from dendrites to the site of action potential initiation. *Type-1* neurons thus appear to be uniquely equipped to promote recurrent excitation and thus periodic burst output, while inhibiting spontaneous excitatory input during interburst intervals.

Over 20 years ago, dendrites were predicted to contain intrinsic membrane conductances necessary for amplification of synaptic input in rhythmically neurons of the preBötC . Nearly 10 years ago, amplification of synaptic input was directly linked to metabotropic glutamate receptors in dendrites (Pace and Del Negro, 2008; Pace et al., 2007). Synaptic integration occurring on dendrites has since been observed and measured in the context of rhythmic activity (Del Negro et al., 2011). However, the subcellular distribution of currents in rhythmically neurons has until now been undefined. The manner in which *specific* ionic membrane currents in dendrites (e.g.,  $I_A$ ) might interact with excitatory events known to also occur in dendrites (e.g. drive amplification) has similarly not been

tested. While the experiments performed here speculate upon the likely interactions occurring in dendrites due to  $I_A$  (i.e. excitatory inhibition), the effects of  $I_A$  on excitatory input in other systems have been documented (Hoffman et al., 1997; Magee, 2000; Magee et al., 1998). For instance, dendritic  $I_A$  in Purkinje neurons is modulated via group I mGluRs and inhibits calcium spiking by high-voltage-activated calcium channels. These calcium spikes evoke bursts of action potentials recorded at the soma (Otsu et al., 2014). Although amplifying currents on dendrites in rhythmically preBötC neurons appear to be activated by a non-specific cation current ( $I_{CAN}$ ), group I mGluRs do indeed promote drive amplification (Pace and Del Negro, 2008), and co-localize with  $I_A$  as demonstrated here. Experiments involving repetitive excitation (i.e. trains of single EPSPs) or dendritic glutamate application, both paired with blockade of  $I_A$  localized to dendrites, could confirm that  $I_A$ , in its deinactivated state, can diminish the effects of sparse excitatory inputs. Additional pharmacology could likewise test whether mGluRs interact with  $I_A$ .

Broadly speaking, the experiments in Chapter 2 highlight the complexity of integrative processes occurring in rhythmically active neurons. Moreover, this may not be exclusive to *type-1* neurons. The hyperpolarization-activated inward current ( $I_h$ ) is prominently featured in *type-2* neurons (Picardo et al., 2013; Rekling et al., 1996), is known to be expressed on dendrites (Lörincz et al., 2002; Notomi and Shigemoto, 2004), and could likewise inhibit temporal summation of excitatory input (Magee, 1998; Stuart and Spruston, 1998; Williams and Stuart, 2000).

The organotypic culture model of inspiratory rhythm generation presented here recapitulates the behavior of acute *in vitro* preparations, provides a means by which experimenters can observe integrative processes occurring on dendrites and additionally lengthens the time-scale on which experiments can be conducted. This in turn permits future use of genetically encoded molecular tools such as protein indicators (e.g. calcium or voltage sensors) and light-activated ion channels (e.g. channelrhodopsins) that can be expressed in a cell- or region-specific manner. As proof of its utility, the culture model here has permitted investigation of integrative properties in dendrites of *type-1* neurons, first predicted over 20 years ago. Until now, these properties were evidenced to exist, but only by indirect means or methods that could not elaborate in detail on the interactions of underlying active membrane currents. Here we show how  $I_A$  can influence the behavior of *type-1* neurons through inhibition of membrane depolarization on their dendrites, which helps to reinforce their putative role as reliable rhythm initiators and provides valuable insight about the neural control of respiratory rhythm.

## REFERENCES

- Arsenault, J., Nagy, A., Henderson, J.T., and O'Brien, J.A. (2014). Regioselective Biolistic Targeting in Organotypic Brain Slices Using a Modified Gene Gun. *J. Vis. Exp. JoVE*.
- Bouvier, J., Thoby-Brisson, M., Renier, N., Dubreuil, V., Ericson, J., Champagnat, J., Pierani, A., Chédotal, A., and Fortin, G. (2010). Hindbrain interneurons and axon guidance signaling critical for breathing. *Nat. Neurosci.* *13*, 1066–1074.
- Del Negro, C.A., Morgado-Valle, C., and Feldman, J.L. (2002). Respiratory Rhythm: An Emergent Network Property? *Neuron* *34*, 821–830.
- Del Negro, C.A., Hayes, J.A., and Rekling, J.C. (2011). Dendritic Calcium Activity Precedes Inspiratory Bursts in preBötzinger Complex Neurons. *J. Neurosci.* *31*, 1017–1022.
- Feldman, J.L., Del Negro, C.A., and Gray, P.A. (2013). Understanding the rhythm of breathing: so near, yet so far. *Annu. Rev. Physiol.* *75*, 423–452.
- Forsberg, D., Horn, Z., Tserga, E., Smedler, E., Silberberg, G., Shvarev, Y., Kaila, K., Uhlén, P., and Herlenius, E. (2016). CO<sub>2</sub>-evoked release of PGE<sub>2</sub> modulates sighs and inspiration as demonstrated in brainstem organotypic culture. *eLife* *5*, e14170.
- Funk, G.D., and Greer, J.J. (2013). The rhythmic, transverse medullary slice preparation in respiratory neurobiology: Contributions and caveats. *Respir. Physiol. Neurobiol.* *186*, 236–253.
- Funk, G.D., Smith, J.C., and Feldman, J.L. (1994). Development of thyrotropin-releasing hormone and norepinephrine potentiation of inspiratory-related hypoglossal motoneuron discharge in neonatal and juvenile mice in vitro. *J. Neurophysiol.* *72*, 2538–2541.
- Gray, P.A., Rekling, J.C., Bocchiaro, C.M., and Feldman, J.L. (1999). Modulation of Respiratory Frequency by Peptidergic Input to Rhythmogenic Neurons in the PreBötzinger Complex. *Science* *286*, 1566–1568.
- Gray, P.A., Hayes, J.A., Ling, G.Y., Llona, I., Tupal, S., Picardo, M.C.D., Ross, S.E., Hirata, T., Corbin, J.G., Eugénin, J., et al. (2010). Developmental

- origin of preBötzinger complex respiratory neurons. *J. Neurosci. Off. J. Soc. Neurosci.* 30, 14883–14895.
- Hoffman, D.A., Magee, J.C., Colbert, C.M., and Johnston, D. (1997). K<sup>+</sup> channel regulation of signal propagation in dendrites of hippocampal pyramidal neurons. *Nature* 387, 869–875.
- Kleinfeld, D., Deschênes, M., Wang, F., and Moore, J.D. (2014). More than a rhythm of life: breathing as a binder of orofacial sensation. *Nat. Neurosci.* 17, 647–651.
- Lörincz, A., Notomi, T., Tamás, G., Shigemoto, R., and Nusser, Z. (2002). Polarized and compartment-dependent distribution of HCN1 in pyramidal cell dendrites. *Nat. Neurosci.* 5, 1185–1193.
- Magee, J.C. (1998). Dendritic Hyperpolarization-Activated Currents Modify the Integrative Properties of Hippocampal CA1 Pyramidal Neurons. *J. Neurosci.* 18, 7613–7624.
- Magee, J.C. (2000). Dendritic integration of excitatory synaptic input. *Nat. Rev. Neurosci.* 1, 181–190.
- Magee, J., Hoffman, D., Colbert, C., and Johnston, D. (1998). Electrical and Calcium Signaling in Dendrites of Hippocampal Pyramidal Neurons. *Annu. Rev. Physiol.* 60, 327–346.
- Moore, J.D., Deschênes, M., Furuta, T., Huber, D., Smear, M.C., Demers, M., and Kleinfeld, D. (2013). Hierarchy of orofacial rhythms revealed through whisking and breathing. *Nature* 497, 205–210.
- Moore, J.D., Kleinfeld, D., and Wang, F. (2014). How the brainstem controls orofacial behaviors comprised of rhythmic actions. *Trends Neurosci.* 37, 370–380.
- Murphy, R.C., and Messer, A. (2001). Gene Transfer Methods for CNS Organotypic Cultures: A Comparison of Three Nonviral Methods. *Mol. Ther.* 3, 113–121.
- Nguyen, T.D., Wirblich, C., Aizenman, E., Schnell, M.J., Strick, P.L., and Kandler, K. (2012). Targeted single-neuron infection with rabies virus for transneuronal multisynaptic tracing. *J. Neurosci. Methods* 209, 367–370.

- Notomi, T., and Shigemoto, R. (2004). Immunohistochemical localization of Ih channel subunits, HCN1–4, in the rat brain. *J. Comp. Neurol.* *471*, 241–276.
- Otsu, Y., Marcaggi, P., Feltz, A., Isope, P., Kollo, M., Nusser, Z., Mathieu, B., Kano, M., Tsujita, M., Sakimura, K., et al. (2014). Activity-dependent gating of calcium spikes by A-type K<sup>+</sup> channels controls climbing fiber signaling in Purkinje cell dendrites. *Neuron* *84*, 137–151.
- Pace, R.W., and Del Negro, C.A. (2008). AMPA and metabotropic glutamate receptors cooperatively generate inspiratory-like depolarization in mouse respiratory neurons in vitro. *Eur. J. Neurosci.* *28*, 2434–2442.
- Pace, R.W., Mackay, D.D., Feldman, J.L., and Del Negro, C.A. (2007). Inspiratory bursts in the preBötzinger complex depend on a calcium-activated non-specific cation current linked to glutamate receptors in neonatal mice. *J. Physiol.* *582*, 113–125.
- Picardo, M.C.D., Weragalaarachchi, K.T.H., Akins, V.T., and Del Negro, C.A. (2013). Physiological and morphological properties of Dbx1-derived respiratory neurons in the pre-Bötzinger complex of neonatal mice. *J. Physiol.* *591*, 2687–2703.
- Ramirez, J.M., Quellmalz, U.J., and Richter, D.W. (1996). Postnatal changes in the mammalian respiratory network as revealed by the transverse brainstem slice of mice. *J. Physiol.* *491*, 799–812.
- Rathenberg, J., Nevian, T., and Witzemann, V. (2003). High-efficiency transfection of individual neurons using modified electrophysiology techniques. *J. Neurosci. Methods* *126*, 91–98.
- Rekling, J.C., and Feldman, J.L. (1998). PREBÖTZINGER COMPLEX AND PACEMAKER NEURONS: Hypothesized Site and Kernel for Respiratory Rhythm Generation. *Annu. Rev. Physiol.* *60*, 385–405.
- Rekling, J.C., Champagnat, J., and Denavit-Saubie, M. (1996). Electroresponsive properties and membrane potential trajectories of three types of inspiratory neurons in the newborn mouse brain stem in vitro. *J. Neurophysiol.* *75*, 795–810.
- Smith, J.C., Ellenberger, H.H., Ballanyi, K., Richter, D.W., and Feldman, J.L. (1991). Pre-Bötzinger Complex: A Brainstem Region That May Generate Respiratory Rhythm in Mammals. *Science* *254*, 726–729.

- Stuart, G., and Spruston, N. (1998). Determinants of Voltage Attenuation in Neocortical Pyramidal Neuron Dendrites. *J. Neurosci.* *18*, 3501–3510.
- Suzue, T. (1984). Respiratory rhythm generation in the in vitro brain stem-spinal cord preparation of the neonatal rat. *J. Physiol.* *354*, 173–183.
- Tan, W., Janczewski, W.A., Yang, P., Shao, X.M., Callaway, E.M., and Feldman, J.L. (2008). Silencing preBötzinger complex somatostatin-expressing neurons induces persistent apnea in awake rat. *Nat. Neurosci.* *11*, 538–540.
- Wickersham, I.R., Lyon, D.C., Barnard, R.J.O., Mori, T., Finke, S., Conzelmann, K.-K., Young, J.A.T., and Callaway, E.M. (2007). Monosynaptic Restriction of Transsynaptic Tracing from Single, Genetically Targeted Neurons. *Neuron* *53*, 639–647.
- Williams, S.R., and Stuart, G.J. (2000). Site Independence of EPSP Time Course Is Mediated by Dendritic  $h$  in Neocortical Pyramidal Neurons. *J. Neurophysiol.* *83*, 3177–3182.